1-1-2017

Project Amiga: A Minimal Covering Factor For Optically Thick Circumgalactic Gas Around The Andromeda Galaxy

J. Christopher Howk

Christopher B. Wotta

D. J. Pisano

S. A. Wolfe

Draft version July 31, 2018
Preprint typeset using LaTeX style AASTeX6 v. 1.0

PROJECT AMIGA: A MINIMAL COVERING FACTOR FOR OPTICALLY THICK CIRCUMGALACTIC GAS AROUND THE ANDROMEDA GALAXY

J. Christopher Howk[1,2], Christopher B. Wotta[1], Michelle A. Berg[1], Nicolas Lehner[1], Felix J. Lockman[3], Zachary Hafen[4], D.J. Pisano[5,6], Claude-André Faucher-Giguère[4], Bart P. Wakker[7], J. Xavier Prochaska[8,9] Spencer A. Wolfe[5,6], Joseph Ribaudo[10], Kathleen A. Barger[11], Lauren Corlies[12], Andrew J. Fox[13], Puragra Guhathakurta[8,9], Edward B. Jenkins[14], Jason Kalirai[12,13], John M. O'Meara[15], Molly S. Peeples[12,13], Kyle R. Stewart[16] Jay Strader[17]

[1]Department of Physics, University of Notre Dame, Notre Dame, IN, USA
[2]Visiting professor, Instituto de Astrofísica, Pontificia Universidad Católica de Chile, Santiago, Chile
[3]Green Bank Observatory, Green Bank, WV, USA
[4]Department of Physics and Astronomy and Center for Interdisciplinary Exploration and Research in Astrophysics (CIERA), Northwestern University, Evanston, IL, USA
[5]Department of Physics & Astronomy, West Virginia University, Morgantown, WV, USA
[6]Center for Gravitational Waves and Cosmology, West Virginia University, Chestnut Ridge Research Building, Morgantown, WV, USA
[7]Department of Astronomy, University of Wisconsin-Madison, Madison, WI, USA
[8]Department of Astronomy and Astrophysics, University of California, Santa Cruz, CA, USA
[9]University of California Observatories, Lick Observatory, Santa Cruz, CA, USA
[10]Department of Physics, Utica College, Utica, NY, USA
[11]Department of Physics & Astronomy, Texas Christian University, Fort Worth, TX, USA
[12]Department of Physics and Astronomy, Johns Hopkins University, Baltimore, MD, USA
[13]Space Telescope Science Institute, Baltimore, MD, USA
[14]Princeton University Observatory, Princeton, NJ, USA
[15]Department of Chemistry and Physics, Saint Michael's College, Colchester, VT, USA
[16]Department of Mathematical Sciences, California Baptist University, 8432 Magnolia Ave., Riverside, CA, USA
[17]Department of Physics and Astronomy, Michigan State University, East Lansing, MI, USA

ABSTRACT

We present a deep search for H I 21-cm emission from the gaseous halo of Messier 31 as part of Project AMIGA, a large Hubble Space Telescope program to study the circumgalactic medium of the Andromeda galaxy. Our observations with the Robert C. Byrd Green Bank Telesope target sight lines to 48 background AGNs, more than half of which have been observed in the ultraviolet with the Cosmic Origins Spectrograph, with impact parameters $25 \lesssim \rho \lesssim 330$ kpc ($0.1 \lesssim \rho/R_{\rm vir} \lesssim 1.1$). We do not detect any 21-cm emission toward these AGNs to limits of N(H I) $\approx 4 \times 10^{17}$ cm^{-2} (5σ; per 2 kpc diameter beam). This column density corresponds to an optical depth of ~ 2.5 at the Lyman limit; thus our observations overlap with absorption line studies of Lyman limit systems at higher redshift. Our non-detections place a limit on the covering factor of such optically-thick gas around M31 to $f_c < 0.051$ (at 90% confidence) for $\rho \leq R_{\rm vir}$. While individual clouds have previously been found in the region between M31 and M33, the covering factor of strongly optically-thick gas is quite small. Our upper limits on the covering factor are consistent with expectations from recent cosmological "zoom" simulations. Recent COS-Halos ultraviolet measurements of H I absorption about an ensemble of galaxies at $z \approx 0.2$ show significantly higher covering factors within $\rho \lesssim 0.5 R_{\rm vir}$ at the same N(H I), although the metal ion-to-H I ratios appear to be consistent with those seen in M31.

Keywords: galaxies: halos – galaxies: individual (M31) – Local Group – quasars: absorption lines

1. INTRODUCTION

The gaseous circumgalactic medium (CGM) around galaxies serves as a massive reservoir of baryons and metals (Peeples et al. 2014; Werk et al. 2014; Keeney et al. 2017) and an import driver of galactic evolution. For example, gas and metals accreted from the CGM may provide the fuel for as much as half of a massive galaxy's stellar mass by $z \sim 0$

(e.g., Oppenheimer et al. 2010; Ford et al. 2014; Anglés-Alcázar et al. 2016). The CGM includes contributions from a broad range of sources. It includes material ejected from the central galaxy in the form of winds (e.g., Weiner et al. 2009; Tripp et al. 2011; Shen et al. 2013; Rubin et al. 2014; Faucher-Giguère et al. 2015; Muratov et al. 2017), which may ultimately return to the galaxy. The CGM includes matter removed from satellites as gas stripped via tidal forces or ram pressure (Grcevich & Putman 2009; Spekkens et al. 2014; Emerick et al. 2016) or gas ejected via the winds of those same satellites (e.g., Anglés-Alcázar et al. 2016).[1] It likely also includes matter that has accreted from the IGM, either as cold gas or gas that is heated via its interaction with the existing CGM (Kereš et al. 2005; Fumagalli et al. 2011a; van de Voort et al. 2011; Faucher-Giguère & Kereš 2011). Most of these processes produce (at least initially) relatively dense, cool concentrations of gas. This is the case even for galactic winds, for which a significant fraction of the mass ejected may come from cool, entrained or condensed material (e.g., Heckman et al. 1990; Schwartz & Martin 2004; Rupke et al. 2005; Rubin et al. 2014; Kacprzak et al. 2014). These cool streams of matter may ultimately fall onto the central galaxy itself, perhaps fueling future star formation (Kereš et al. 2005; Oppenheimer et al. 2010; Ford et al. 2014) or dissipate within the hotter, more diffuse coronal matter in the halo (e.g., Joung et al. 2012; Voit et al. 2015). Thus, the observable CGM about galaxies is expected to be multiphase, with the very diffuse warm and hot gas ($10^5 \lesssim T \lesssim 10^7$ K; Tumlinson et al. 2011; Prochaska et al. 2011; Wakker & Savage 2009; Anderson et al. 2013) threaded with denser cool gas ($10^4 \lesssim T \lesssim 10^5$ K; Nielsen et al. 2013; Kacprzak et al. 2013; Werk et al. 2014; Keeney et al. 2017), including the dense structures that could represent new matter flowing into the CGM for the first time (Lehner et al. 2013; Wotta et al. 2016; van de Voort et al. 2012).

In the context of the CGM, such dense ($n_{\rm H} \gtrsim 10^{-3}$ cm^{-3}) and cool ($T < 10^5$ K) structures are ionized entities. They have characteristic densities and size scales that produce optical depths at the Lyman limit of order unity and above (Schaye 2001; Fumagalli et al. 2011b; Faucher-Giguère & Kereš 2011; van de Voort et al. 2012). In QSO absorption line studies of the CGM, these streams would thus be categorized as Lyman limit systems (LLSs; Tytler 1982; Steidel 1990), with H I column densities $N({\rm H\,I}) \geq 1.6 \times 10^{17}$ cm^{-2} ($\log N({\rm H\,I}) \geq 17.2$), which corresponds to an optical depth at the H ionization edge of $\tau_{\rm 1Ryd} \geq 1$ (Spitzer 1978). Studies of low-redshift Lyman limit systems have shown they exhibit a broad range of metallicities, from $< 1\%$ solar to super-solar metallicities (Lehner et al. 2013; Wotta et al. 2016), as expected if they are tracing a range of origins, including accreting, stripped, or expelled matter.

Simulations of galaxies at $z \approx 2$ show that optically-thick H I material may cover $\sim 2\% - 10\%$ of the area within the virial radius of typical galaxies (e.g., Fumagalli et al. 2011b; Faucher-Giguère & Kereš 2011), with a signicantly higher covering fraction at the smallest impact parameters. Only recently have simulations been able to regularly study the high-density structures in the CGM to $z = 0$ with full feedback prescriptions. The covering factors of optically thick gas in simulated galaxies at low redshift tend to be lower on average than their higher-redshift counterparts, partly due to the general dimunition expected in cold accretion as well as generally diminished feedback. For example, Hafen et al. 2017 (hereafter H17) find a median $f_c \sim 1\%$ for $\log M_{\rm halo}/M_\odot \approx 12$ galaxies at $z = 0$. Still, the covering factors for individual galaxies can be as high as $f_c \sim 10\% - 15\%$, depending on the feedback recipes and the histories of recent star formation, mergers, and accretion (Gutcke et al. 2016, H17). Measurements of optically-thick H I thus constrain the total mass in the densest material associated flows of matter through the CGM while also constraining prescriptions for feedback and other processes in galaxy simulations.

The study of galactic halos at $\log N({\rm H\,I}) \sim 17 - 18$ has largely been limited to absorption line measurements. However, the the best radio observatories now reach sensitivities to H I 21-cm emission that get nearly to $\tau_{\rm 1\,Ryd} \approx 1$ gas around low-redshift galaxies (e.g., Braun & Thilker 2004; Lockman et al. 2012; Wolfe et al. 2013, 2016), bridging the gap between emission and absorption experiments. Radio searches for faint emission have the distinct advantage of (potentially at least) providing more spatial information than can be gleaned from the small numbers of skewers that are available for absorption line spectroscopy, with its need for bright background sources (especially in the ultraviolet).

Here we use the Robert C. Byrd Green Bank Telescope (GBT), part of the Green Bank Observatory,[2] to search for 21-cm emission from the halo of the nearby Andromeda galaxy. This 21-cm search is in support of our Project AMIGA (Absorption Maps In the Gas of Andromeda)[3], a large *Hubble Space Telescope* (*HST*) program to study the absorption from the extended CGM about the Andromeda galaxy (M31) using the Cosmic Origins Spectrograph (COS). Project AMIGA will measure UV absorption lines along ∼25 AGN sight lines passing within $\rho \approx R_{\rm vir} \approx 300$ kpc of the center of M31. This builds on our recent study demonstrating that M31 has a massive, diffuse CGM

[1] These are not necessarily mutually exclusive, as ram pressure may play a role in removing wind-driven matter from the satellite's halo.

[2] The Green Bank Observatory is a facility of the National Science foundation operated under a cooperative agreement by Associated Universities, Inc.

[3] Not to be confused with the AMIGA survey (Analysis of the interstellar Medium in Isolated GAlaxies, PI Lourdes Verdes-Montenegro); `http://amiga.iaa.es`.

stretching to approximately $R_{\rm vir}$ (Lehner et al. 2015, hereafter LHW15). Project AMIGA will characterize the radial and azimuthal dependences of metal ion surface densities (for C II, C IV, Si II Si III, Si IV, and others) in M31's CGM. However, our *HST* observations will provide little information on the H I distribution at the velocities where LHW15 find metal absorption from M31's CGM ($v_{\rm LSR} \gtrsim -500$ km s^{-1}), as the strongly-saturated Lyα absorption from the Milky Way completely blocks the light from the background AGNs over these wavelengths. This is not a problem with H I emission, where the Milky Way emission is largely constrained to higher velocities than M31's CGM.

In the present work we target 48 directions through the Andromeda galaxy's halo in order to measure the covering factor of highly optically-thick gas ($\tau_{1\,\rm Ryd} \approx 2.5$). Our observations achieve sensitivities to H I column densities that overlap with absorption line measurements of CGM H I about more distant galaxies (e.g., Tumlinson et al. 2013; Lehner et al. 2013; Prochaska et al. 2017) and UV absorption line studies of high-velocity clouds in the CGM of our own Milky Way (e.g., Fox et al. 2006). As the 21-cm line is so easy to excite (the critical density for excitation is $n_{\rm crit} \approx 3 \times 10^{-5}$ cm^{-3}, well below the density of gas we are considering, and Lyα pumping is also an effective excitation mechanism), these GBT observations allow us to trace gas even in conditions expected of the CGM.

There is good reason to suspect that M31 may have a significant CGM, even one detectable in 21-cm emission. The relative dearth of neutral gas associated with dwarf satellite galaxies has led several groups to to argue for the existence of a low-density diffuse CGM about M31 to impact parameters $\rho \lesssim 270$ kpc (Blitz & Robishaw 2000; Grcevich & Putman 2009, see also Spekkens et al. 2014 for similar work specific to the Milky Way). Similarly, although the giant southern stream has a dynamical age of < 1 Gyr (Fardal et al. 2008), its star formation was shut off well before it was tidally disrupted ($\gtrsim 4$ Gyr ago; Brown et al. 2006), suggesting its gas was stripped by M31's CGM long ago. Grcevich & Putman used ram pressure stripping arguments to imply a density of a few $\times 10^{-4}$ cm^{-3} for a diffuse (potentially hot) corona about M31. Rao et al. (2013) searched for metal line absorption from the halo of M31, but their sensitivity was limited by the low spectral resolution of their data. LHW15 found significant metal ion surface densities for sight lines projected within $\rho \approx R_{\rm vir} \approx 300$ kpc of M31, suggesting an extended distribution of low-density gas. The total CGM gas mass implied by the LHW15 observations is significant at $M_{\rm total} \gtrsim 2 \times 10^8\,(Z/Z_\odot)^{-1}\ M_\odot$ within $0.2R_{\rm vir}$, although the total mass could be a factor of 10 larger if the covering factor is near unity to the virial radius.[4]

The H I emission from the diffuse CGM implied by these studies may be minimal, depending on the metallicity and ionization state of the gas. In the Andromeda system, Braun & Thilker (2004) reported the detection of a diffuse "bridge" of low column density material stretching between M31 and its companion M33 (projected ~ 200 kpc from M31), with an extension several degrees beyond M31 in the north ($1^\circ \approx 13$ kpc at M31). In total Braun & Thilker found the filament stretched nearly 260 kpc. This work was done with a coarse angular resolution of $49'$ and velocity resolution of 18 km s^{-1} to achieve a sensitivity of $\log N({\rm H\,I}) \approx 17$ for emission filling the beam, and much of the bridge emission appeared to have beam-averaged column densities well below $\log N({\rm H\,I}) \sim 18$. Subsequent high-resolution maps of the vicinity of M33 have called into questioned the presence of this bridge, given the lack of a bridge component in the maps of M33 (Putman et al. 2009). Lockman et al. (2012) confirmed the existence of faint 21-cm emission in this region between the two galaxies, but they noted the gas must be very patchy, as they did not find it consistently over several GBT pointings. Wolfe et al. (2013) and Wolfe et al. (2016) showed that most of the emission identified by Braun & Thilker (2004) was associated with higher column density, small-scale clumps of gas. The "bridge" appears to be constituted of small clouds (each with masses $\sim 10^5\ M_\odot$) that appeared as more continuous, diffuse structure when diluted within the Westerbork beam employed by the Braun & Thilker study. And while Wolfe et al. (2016) did detect some emission in the extended structure found by Braun & Thilker (2004) to the northwest of M31, the spatial distribution of this gas appears to be much different than that implied by the initial maps. Thus, M31's CGM appears to harbor at least some small-scale concentrations of H I detectable through their 21-cm emission.

In the inner regions of M31's halo, Thilker et al. (2004) identified a population of high-velocity clouds (HVCs) projected within $\rho \sim 50$ kpc of the center of M31, which were subsequently mapped at higher resolution by Westmeier et al. (2005). These clouds individually have H I masses $M_{\rm HI} \approx 10^5 - 10^6\ M_\odot$ with size scales of ~ 1 kpc and central column densities $N({\rm H\,I}) \sim 10^{19}$ cm^{-2} (Westmeier et al. 2005). They are discrete structures, dense clouds ($n_{\rm HI} \approx 10^{-2}$ cm^{-3}) in the CGM that may be similar to the clouds identified at larger distances by Wolfe et al. (2016), though with higher masses.

In the present experiment (Project AMIGA GBT), we survey sight lines toward UV-bright AGNs with impact parameters $\rho \lesssim R_{\rm vir}$ from M31 in order to characterize the distribution of dense, cool gas in the CGM. In no cases have

[4] The results initially given in LHW15 are too high by a factor of ~ 10 due to an unfortunate error.

the observed directions been chosen with prior knowledge of the local H I content. Thus, we can use our observations to directly determine the covering factor of optically-thick gas in the CGM of M31. Our covering factor estimates are complementary to the Richter (2012) assessment of the covering factor of HVCs about M31 based on the Thilker et al. (2004) maps (which have a 5σ column density sensitivity of $\log N(\mathrm{H\,I}) \sim 18.25$ per GBT beam for a FWHM= 25 km s^{-1}, significantly higher than our observations).[5]

Our paper is presented as follows. We summarize the GBT observations and data reduction in §2. We derive covering factors for cool gas about the Andromeda galaxy in §3. In §4 we consider the covering factor results in the context of recent QSO absorption line measurements and numerical simulations. Our discussion and summary follow in §5 and §6. A metallicity measurement for a sight line passing through the nearby Magellanic Stream (MS) is included in an Appendix.

Throughout we assume a distance of 752 kpc to M31 (Riess et al. 2012). For comparison with other galaxies (simulated and observed), we assume for M31 a stellar mass $\log M_*/M_\odot \approx 11.0$ and a halo mass $\log M_\mathrm{h}/M_\odot \approx 12.0$ (Tamm et al. 2012).

2. GBT 21-CM OBSERVATIONS AND ANALYSIS

We used the 100-m diameter Robert C. Byrd Green Bank Telescope (Prestage et al. 2009) to take pointed observations toward 48 AGNs projected behind the CGM of M31 as part of NRAO programs GBT15A-328 and GBT14B-436. A map showing the locations of the AGNs is given in Figure 1, and the details of the AGN sight lines are summarized in Table 1. These sight lines represent two samples that, together, should provide an unbiased sampling of the H I content of the Andromeda galaxy's gaseous halo. The first sample consists of 25 objects in the Project AMIGA sample, shown with red outlines in Figure 1. These are selected to be UV-bright AGNs projected within $\rho \approx 340$ kpc ($\sim 1.1 R_\mathrm{vir}$) of the center of M31. They are chosen to probe a broad range of impact parameters, with sight lines focused about the major axis, minor axis, and intermediate orientations. They do not sample the impact parameter space randomly (i.e., with weighting $\propto \rho^2$). Furthermore, they do not randomly sample the azimuthal distribution, both because of the goals of Project AMIGA (to probe the azimuthal variations systematically) and of a general dearth of identified UV-bright AGNs behind the northern half of M31's CGM (see LHW15).

The remaining 23 pointings (shown with black outlines in Figure 1) sample sight lines toward UV-bright AGNs (and one blank sky direction) that are not scheduled for *HST* observations. These supplemental sight lines were chosen because they may eventually represent quality target for UV follow-up, and because they provide an expansion of our survey in a way that mimics the initial selection. In both cases, the principal criterion for selecting a sight line is the presence of a UV-bright background source. This selection is independent of the H I distribution, and we used no knowledge of the H I structure of M31 in selecting background sources. There is a bias in the distribution of the sources to the southern half of Andromeda's CGM. This is in part due to the increased extinction northward of M31 (at lower Galactic latitudes) and a lack of surveys at those lower latitudes (a result being rectified by QSO searches with, e.g., LAMOST; Huo et al. 2013). We note that if the goal of our program was simply to derive information about the covering factor of low column density H I in the vicinity of M31, we would not need to search in directions toward background AGNs. However, the present program was designed with the UV observations (or potential future observations) in mind, so that deep H I observations might help constrain the metallicity of the CGM viewed in UV absorption.

The pointed GBT observations were taken with the L-band receiver and have a $9\farcm1$ primary beam. Each AGN direction was initially observed for a total of 50–60 minutes in individual 10 minute scans. In a few cases difficulties with the receivers caused one of the polarizations to be unusable. We received additional director's discretionary time (program GBT16A-433) to reobserve 12 of the sight lines. Our observations employed a 5.16 MHz bandwidth centered on the H I hyperfine transition and have a native channel spacing of 0.15 km s^{-1}. The typical system temperature of the GBT in this configuration is 18 K at zenith in both linear polarizations. Our observations are consistent with this expectation, with most values in the range $17.3 \lesssim T_\mathrm{sys} \lesssim 19.0$ K during our observations. The exceptions are those observations taken toward radio-bright AGNs 3C48 (45 K) and 3C59 (21.9 K) as well as the direction toward 3C66A (24.6 K). None of the other background AGNs is within a factor of 10 of the brightness of 3C48 and 3C59 (which have 1.4 GHz fluxes of $\sim$ 16 and 2 Jy). In-band frequency switching (with a throw of 3 MHz) was used for background subtraction. This provided useable velocity coverage of typically $-515 \lesssim v_\mathrm{LSR} \lesssim +470$ km s^{-1}.

We performed the data reduction within GBTIDL (Marganian et al. 2006), following Boothroyd et al. (2011) for

[5] Thilker et al. (2004) discuss several variations of their datacube, each smoothed to different velocity and spatial resolutions. Here we give the limits associated with their higher-resolution data, with a $\approx 13\farcm65$ beam and 18 km s^{-1} velocity channels. Their limits imply a mass sensitivity of $M_\mathrm{H\,I} \leq 3.5 \times 10^4\ M_\odot$ per beam.

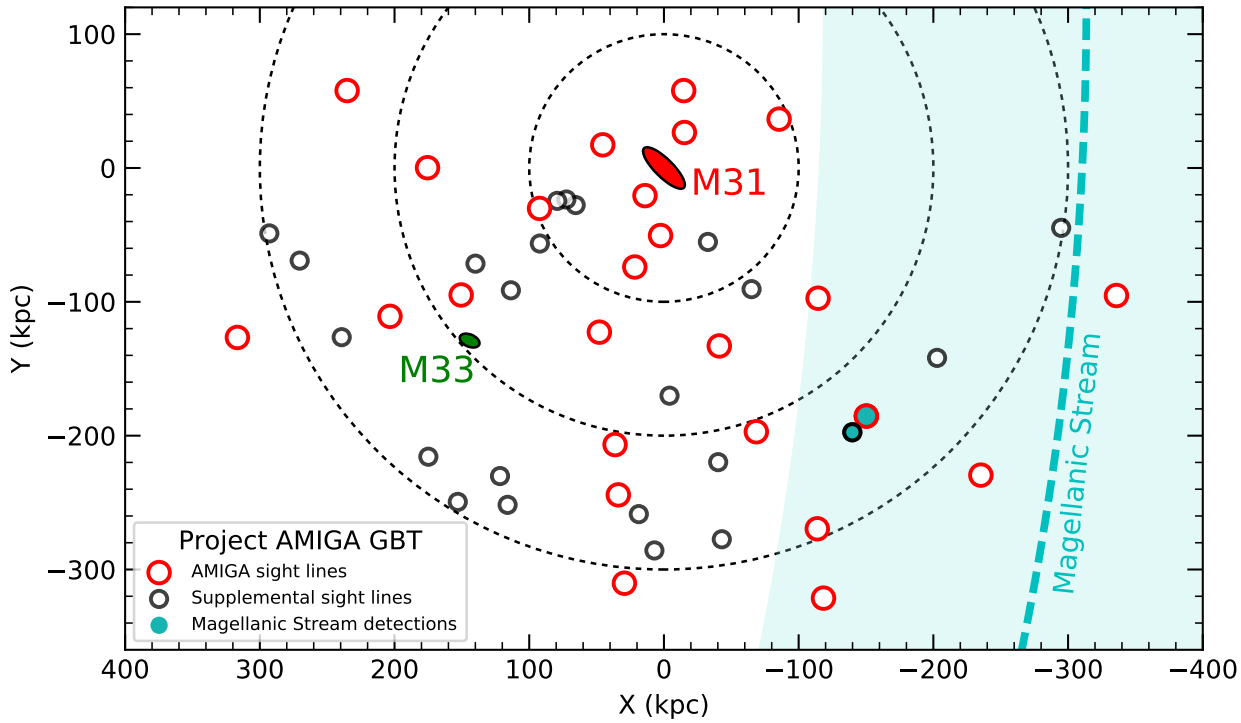

Figure 1. The locations of our GBT pointings relative to the M31-M33 system, where the axes show physical impact parameter from the center of M31. In this orientation, north is up, east to the left. The 25 Project AMIGA sight lines have red outlines; the supplemental sight lines have black outlines and are smaller. Two probable MS detections are filled in cyan. The remainder of the sight lines have non-detections of H I associated with M31. Dotted circles show impact parameters $\rho = 100$, 200, 300 kpc, the last being roughly $R_{\rm vir}$. The sizes and orientations of the two galaxies are taken from the RC3 (de Vaucouleurs et al. 1991) and correspond to the optical R_{25} values. The dashed line shows the plane of the Magellanic System ($b_{\rm MS} = 0°$) as defined by Nidever et al. (2008). The region within $b_{\rm MS} = \pm 15°$ is shaded.

the basic brightness temperature calibration and stray radiation correction and Lockman et al. (2012) for the scan coaddition and baseline fitting. For each sight line we individually examined each 10 minute scan, including both polarizations. In some cases we interpolated over occasional localized interference, i.e., for interference affecting a small number of channels in a given scan. In a few cases, individual scans were excluded from the coaddition if such interference occupied a large number of channels. The quality of the spectral baselines is one of the limiting factors in setting our column density sensitivity. For some scans, one of the linear polarized receivers had much worse baselines than typical. We excluded these from the subsequent data processing. We fitted spectral baselines separately to each scan and linear polarization over a very broad velocity range before coaddition. We adopted third- to fifth-order polynomials, taking care to exclude regions of potential emission from the fitting. The individual baseline-corrected spectra for a given sight line were then coadded with equal weights after applying an atmospheric extinction correction to each. Finally we corrected for the GBT's main beam efficiency at 21-cm ($\eta_{\rm mb} = 0.88$). The final data are binned to ~ 0.6 km s^{-1} channel width. Several examples of our final spectra are shown in Figure 2.

We have performed an automated search for emission at $\geq 5\sigma$ significance over the velocity range $-515 \leq v_{\rm LSR} \leq -170$ km s^{-1} (M31 has a systemic velocity $v_{\rm sys} = -300$ km s^{-1}). Our observations have typical RMS brightness temperature fluctuations of $\sigma_{\rm b} \approx 8$ mK over the search velocities, with a full range between ≈ 7 and 12 mK per 0.6 km s^{-1} channel. The RMS brightness temperatures for each sight line, derived empirically over the full range of velocities searched for M31 emission, are given in Table 1. Because we have calculated these empirically they include both the random noise and the effects of imperfect baseline subtractions or local baseline irregularities.

For each sight line we calculate detection limits for the H I column density assuming the optically thin approximation: $N({\rm H\,I}) = [1.8 \times 10^{18}\ {\rm cm^{-2}}\ ({\rm K\ km\ s^{-1}})^{-1}] \int T_b\, dv$. Any H I in the CGM of M31 will be optically thin in the 21-cm line. The opacity of the 21-cm line is $\tau = (5.2 \times 10^{-19}\ {\rm K\ km\ s^{-1}\ cm^2})\, N({\rm H\,I})\, {\rm FWHM}^{-1}\, T_{ex}^{-1}$ (Dickey & Lockman 1990),

where the excitation temperature is generally close to the kinetic temperature of the H I. Thus for the expected H I column densities $\approx 10^{18}$ cm^{-2}, FWHM = 25 km s^{-1}, and $T_{ex} > 1000$ K, the peak optical depth will be $\tau < 2 \times 10^{-5}$. Although the 21-cm measurements were made toward AGN, these almost always contribute a negligible amount of radio continuum emission. Even for the exception, 3C48, which has a continuum antenna temperature ~ 30 K at the GBT, the continuum temperature is much less than the 21-cm excitation temperature. It would reduce the 21-cm emission line by < 1 mK for the expected 21-cm opacities, a signal that is well below the noise level.

Our detection limits are given in Table 1 based on the RMS brightness temperature fluctuations and an assumed line width of 25 km s^{-1} (FWHM). This yields typical 5σ detection limits of $N(\mathrm{H\,I}) \leq 4 \times 10^{17}$ cm^{-2} per beam or better. Our choice of FWHM is based on the median FWHM in detections of M31 HVC and clump emission from the studies of Thilker et al. (2004), Westmeier et al. (2008), Lockman et al. (2012), and Wolfe et al. (2016). Our typical sensitivity is equivalent to an H I mass of $M_{\rm HI} \sim 10^4\ M_\odot$ per beam ($\sim 800\ M_\odot$/kpc^2), no matter the scale of the emission.

Toward the direction of M31's extended halo, H I emission from gas associated with the Milky Way and its HVCs, the Magellanic Stream (MS), and M31 can overlap in velocity, as discussed in detail by several works (Thilker et al. 2004, LHW15, Kerp et al. 2016). M31 itself has a systemic velocity in the LSR frame $v_{\rm LSR}(\mathrm{M31}) = -300 \pm 4$ km s^{-1}, and we expect potential CGM emission within $\sim \pm 225$ km s^{-1} of the systemic velocity, given that more than 90% of the candidate dwarf galaxies in the M31 system lie within this range (McConnachie 2012). The upper velocity limit for our search is set by the likelihood of contamination by emission from relatively local Galactic HVCs, which are confined to $v_{\rm LSR} \gtrsim -170$ km s^{-1} (Lehner & Howk 2011; Lehner et al. 2012, LHW15). The lower velocity limit corresponds to the limits of the M31 HVC emission found by Thilker et al. (2004). None of the emission detected in high-fidelity GBT individual pointings or maps (Thilker et al. 2004; Lockman et al. 2012; Wolfe et al. 2013, 2016) have found emission at velocities more negative than $v_{\rm LSR} = -515$ km s^{-1}; neither have absorption line searches for gas associated with the Andromeda galaxy (LHW15, Rao et al. 2013). In addition, most of our spectra do not give access to velocities more negative than $v_{\rm LSR} \lesssim -515$ km s^{-1} given the adopted frequency-switching offset. At the same time, we can demonstrate that no Lyα absorption exists in the range $-1000 \leq v_{\rm LSR} \leq -600$ km s^{-1} toward the 25 AGNs in the Project AMIGA sample. This is based on a careful search of the blue edge of the Milky Way Lyα damping wings. Given the strength of this line, we would detect any gas with $\log N(\mathrm{H\,I}) \gtrsim 13.5$. This search will be presented in a future paper.

In addition to potential contamination by Milky Way HVCs, the MS crosses through this region of the sky at velocities that contaminate searches for M31 emission, as detailed by LHW15 (see also Nidever et al. 2008; Fox et al. 2014). The emission from the MS is most important at small Magellanic latitudes ($b_{\rm MS}$), although metal ion absorption from the MS can be seen to at least $b_{\rm MS} \approx \pm 30°$ (Fox et al. 2014) and at Magellanic longitudes $l_{\rm MS} \gtrsim -110°$. We show in Figure 1 the position of $b_{\rm MS} = 0°$ as a dashed curve, and we shade the region between $b_{\rm MS} = \pm 15°$. The MS velocities can be predicted following Nidever et al. (2008), as described in detail by LHW15 (see their Figure 3). Such contamination is only important at $v_{\rm LSR} \gtrsim v_{\rm sys}(\mathrm{M31}) \approx -300$ km s^{-1} (de Vaucouleurs et al. 1991).

Significant H I emission over $-515 \leq v_{\rm LSR} \leq -170$ km s^{-1} is observed in only 2 of our 48 sightlines (see Figure 2) at 5σ significance. The sight lines toward RBS 2055 and RBS 2061 (the filled points in Figure 1) show H I emission at the level of $\log N(\mathrm{H\,I}) \sim 17.8$. The H I profiles for these directions are shown in Figure 2, and the line properties are summarized in Table 2. These objects lie only 1.°2 apart on the sky; both directions show emission at $v_{\rm LSR} \approx -336$ km s^{-1}. RBS 2055 and RBS 2061 have Magellanic coordinates $(l_{\rm MS}, b_{\rm MS}) = (-113.2, +11.0)$ and $(-112.1, +11.6)$, respectively. Thus, both sight lines lie close to the great circle on which the Magellanic system resides, and the detected emission has velocities close to those expected for the extrapolation of the MS in these directions. Our Project AMIGA COS observations of the sight line towards RBS 2055 also reveal significant metal line absorption. In particular, and unique among the Project AMIGA sight lines, this sight line shows absorption from O I λ1302 at the same velocity as the H I emission (as well as other metal lines). As we show in the Appendix, the comparison of $N(\mathrm{O\,I})/N(\mathrm{H\,I})$, which gives a good measure of O/H with very small if any ionization corrections, yields a metallicity estimate $[\mathrm{O/H}] = -0.95 \pm 0.12$. This is consistent with the metallicities of the main body of the MS derived by Fox et al. (2010, 2013). This agreement in metallicity with the general MS, and the location of these directions relative to the MS, strongly suggests the detected 21-cm emission arises in the extension of the MS across this region. We will assume these directions probe MS gas at $v_{\rm LSR} \approx -336 \pm 15$ km s^{-1} moving forward. We note that no H I emission is detected in these directions outside of those expected for the MS, although we do find absorption from M31's CGM at velocities distinct from the MS in the strongest lines covered by the Project AMIGA COS data (see the Appendix).

3. H I COLUMN DENSITY AND COVERING FACTOR LIMITS

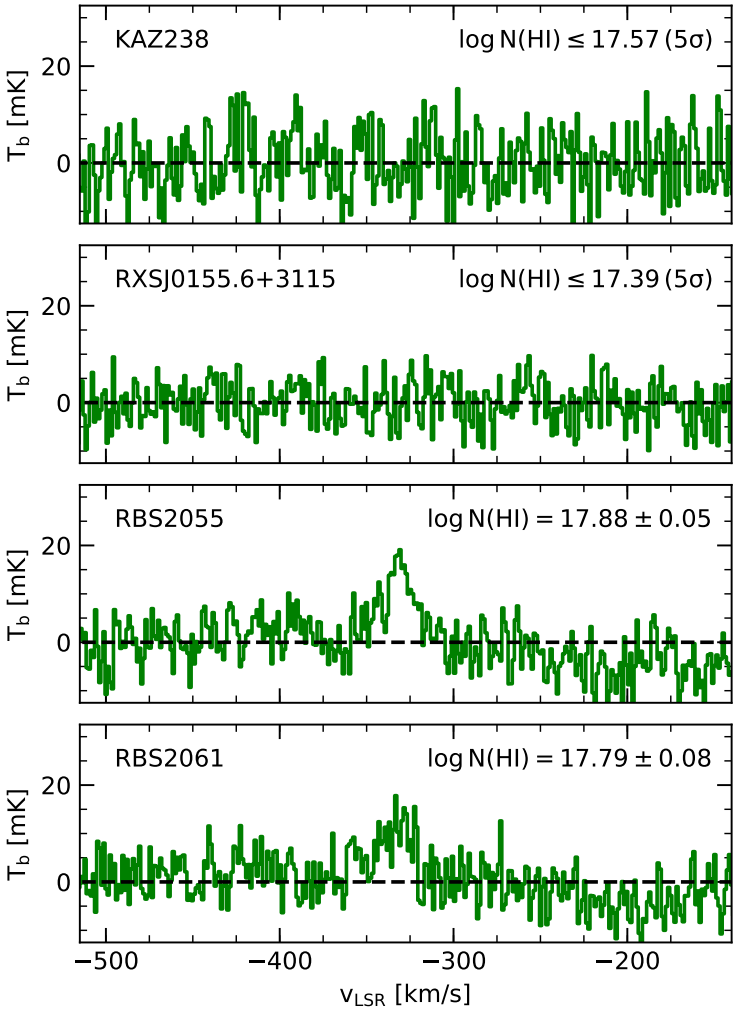

Figure 2. Four spectra from our GBT observations covering the velocity range $-515 \leq v_{\rm LSR} \leq -170$ km s^{-1} (sight line identifications are given in the upper left of each panel). The top two spectra are characteristic examples of the vast majority of the observations, showing no detectable H I 21-cm emission from the CGM of M31. The bottom two spectra show the H I emission observed toward RBS 2055 and RBS 2061 (properties of the lines are given in Table 2). All spectra are shown Hanning-smooted to $\Delta v \approx 1.2$ km s^{-1}. Limits are determined using the RMS brightness temperature variations across the uncontaminated spectral range of the observations and assuming FWHM = 25 km s^{-1}.

We have in hand a sample of 48 pointings through the halo of the Andromeda galaxy at impact parameters $\rho < 1.2R_{\rm vir}$ with sensitivity to H I 21-cm emission of $N({\rm H\,I}) \approx 2 - 4 \times 10^{17}$ cm^{-2} per beam. The N(H I) limits for each sight line are shown as a function of impact parameter in Figure 3 and reported in Table 1. To encompass the range of sensitivites, we adopt a survey search sensitivity of $N({\rm H\,I}) \leq 4 \times 10^{17}$ cm^{-2} ($\log N({\rm H\,I}) \leq 17.60$). The 5σ upper limits are shown for each sight line, with the exception of the two MS detections discussed in §2, for which the detected MS emission column densities are shown. Outside of the velocity range $-370 \lesssim v_{\rm LSR} \lesssim -300$ km s^{-1}, these two sight lines show no emission to limits similar to those observed along the other sight lines (see Table 1).

Clouds with H I column densities $\log N({\rm H\,I}) \geq 17.6$ could be present on scales smaller than the 2 kpc diameter GBT beam and remain undetected, as our limits apply to the beam-averaged column density. Indeed, high-resolution observations of HVCs in the inner regions of the halo ($\rho \lesssim 50$ kpc) by Westmeier et al. (2005) have demonstrated that at least some M31 HVCs have smaller sizes ($\langle D \rangle \sim 1$ kpc) and higher central column densities ($\langle N({\rm H\,I}) \rangle \approx 4 \times 10^{19}$

cm^{-2}). Objects like these specific clouds would be readily detected by our observations on the basis of their masses ($\langle M_{\rm HI}\rangle \approx 10^5\ M_\odot$), but there may still be small-scale clouds that lie below the detection limits of our data. In fact, the photoionization simulations by Lehner et al. (2013) suggested relatively small sizes for the $z \lesssim 1$ LLSs in that work (the vast majority of which have N(H I) $\lesssim 10^{17}$ cm^{-2}), with only 11/25 of the systems they modeled having sizes > 1 kpc. We will discuss this issue further below.

Also shown on Figure 3 are predictions from the recent "zoom-in" galaxy simulations. The blue curve shows the median H I profile from the `ALL_Efb_e001_5ESN` of Liang et al. (2016), which they note best fits recent COS observations of the CGM about $z \lesssim 1$ galaxies while producing "unrealistic" results for the stellar component of a typical low-redshift galaxy. The cyan shading about the line represents the 95% confidence range of the measurements drawn from their simulation. Similar results from the NIHAO simulations of Gutcke et al. (2016) are shown in the dashed lines. These represent the median profiles of their mock H I distributions for individual galaxies with stellar masses $\log M_*/M_\odot = 10.66$ and 10.89, those closest to M31. (Here we do not show the quantiles, but they are similar in magnitude to those shown for the Liang et al. simulations.) The main point in this comparison of both the Liang et al. and Gutcke et al. simulations with our results is that H I about a typical simulated galaxy falls off quite rapidly, save for the filaments and smaller-scale structures tracing flows through the CGM.

The principal result of our work is a calculation of the cumulative covering factor of H I as a function of impact parameter from M31. We calculate the covering factor from our data assuming a binomial distribution. We follow Cameron (2011) in assessing the likelihood function for values of the covering factor, $f_c(\leq \rho)$, given the number of

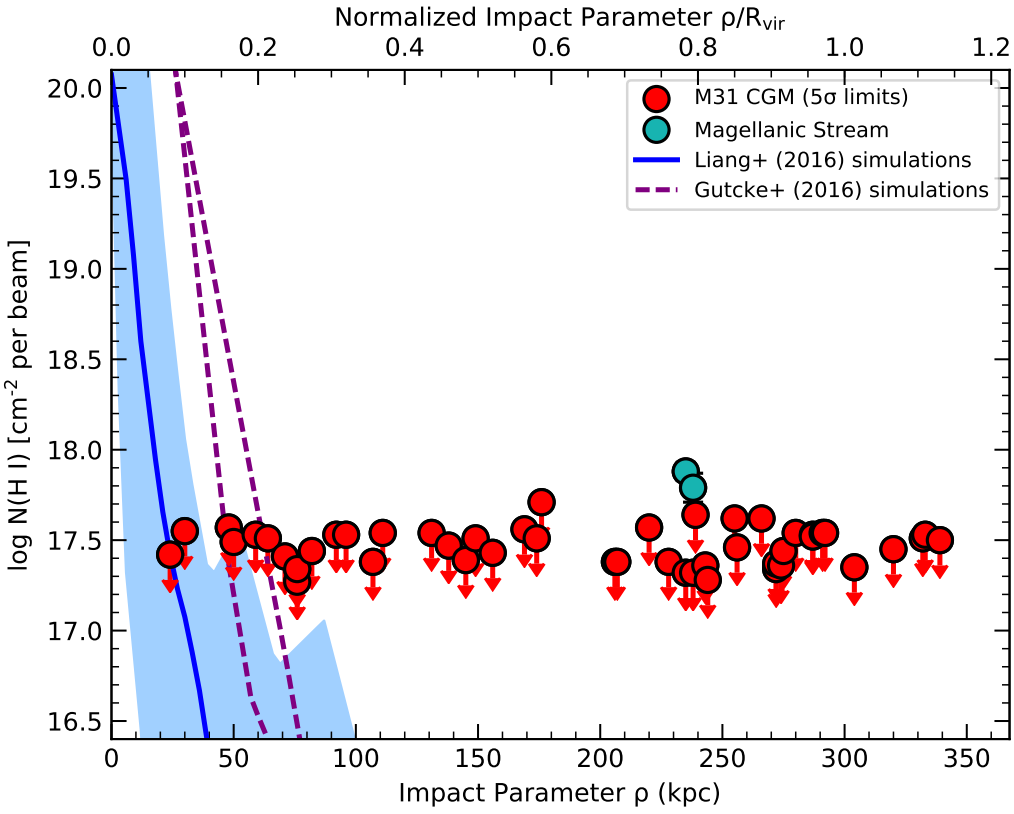

Figure 3. Observed column densities and limits along each of the 48 GBT sight lines through the CGM of M31. Upper limits (red) are given at the 5σ level assuming a FWHM = 25 km s^{-1}. They are determined over a velocity range $-515 \lesssim v_{\rm LSR} \lesssim -170$ km s^{-1}. Two detections of apparent MS emission are shown in cyan. Those two sight lines would have $\log N$(HI) $\lesssim 17.6$ outside of the velocities expected for the MS ($-370 \lesssim v_{\rm LSR} \lesssim -300$ km s^{-1}). Also shown are profiles from recent simulations of H I around massive galaxies. The blue line shows the median H I profile from the $z = 0$ simulation of Liang et al. (2016) that best fits the ensemble of low-redshift CGM observations (their `ALL_Efb_e001_5ESN` run) along with the 95% confidence range of their values (cyan shading). This simulation follows a single $\log M_{\rm h}/M_\odot \sim 12$ halo to $z = 0$; while it does fairly well at matching CGM observations, its stellar component is "unrealistic" (Liang et al. 2016). The dashed lines are examples of results from Gutcke et al. (2016), showing the median values for their $\log M_*/M_\odot = 10.66$ and 10.89 galaxies.

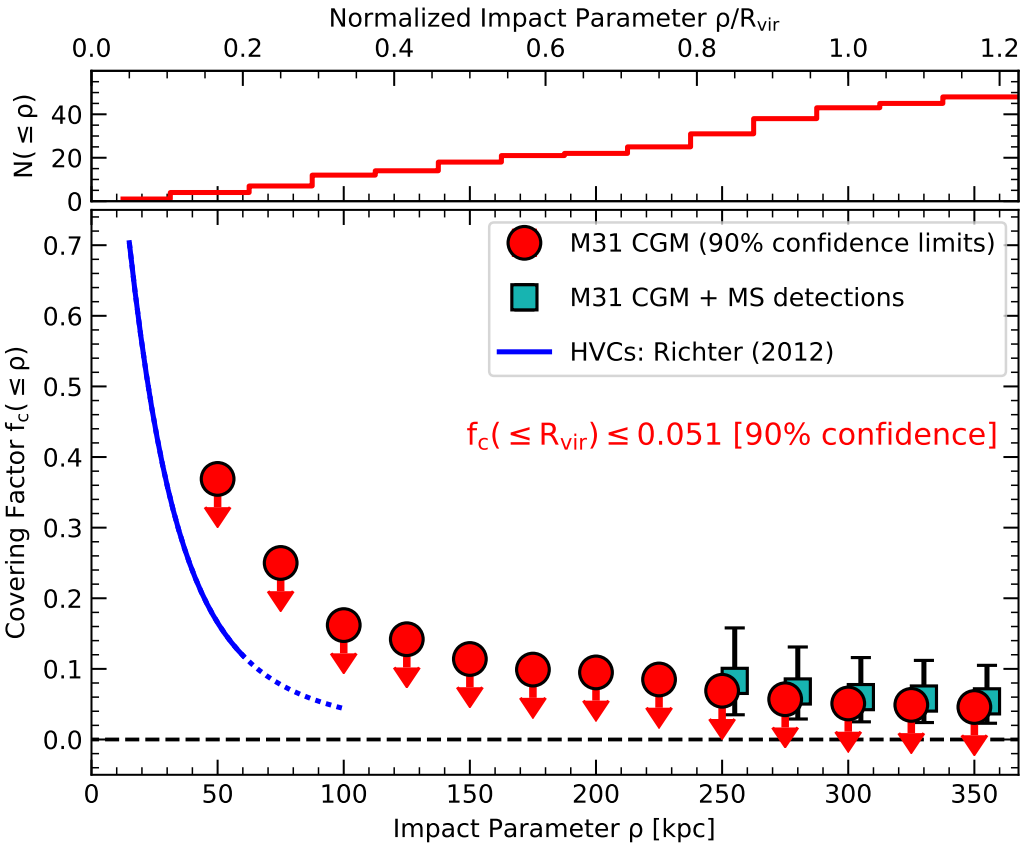

Figure 4. The cumulative covering factors for impact parameters less than ρ, $f_c(\leq \rho)$, from our GBT observations. These values are appropriate for $\log N(\mathrm{HI}) \gtrsim 17.6$ ($N(\mathrm{H\,I}) \gtrsim 4 \times 10^{17}$ cm^{-2}). Upper limits are shown at 90% confidence. We assume a binomial distribution for each bin and follow the approach of Cameron (2011) in calculating the one-sided confidence limit using the incomplete beta function estimator (for a number of targets given in the top panel). The covering factor limit for impact parameters less than the virial radius is $f_c(\leq R_{\rm vir}) \leq 0.051$. Also shown in cyan are the covering factors that would be derived if one assumes the two sight lines with apparent MS emission are instead tracing emission from the CGM of M31 (shifted to slightly larger impact parameter for clarity). The central value is the median of the posterior probability distribution from the beta distribution generator, while the error bars denote the 80% confidence interval (i.e., the 10% and 90% quantiles) (Cameron 2011). The blue line shows the covering factor of HVCs in the inner regions of the halo (limiting sensitivity of $\log N(\mathrm{H\,I}) \sim 18.25$), adjusting the results of Richter (2012) to reflect a cumulative covering factor.

detections (successes) against the total sample (number of sight lines within a given impact parameter). Cameron demonstrates that the normalized likelihood function useful for calculating (Bayesian) confidence intervals on a binomial distribution with a non-informative (uniform) prior follows a beta distribution. We refer the reader to Cameron (2011) for a detailed justification of this approach, which is particularly useful for providing robust results in cases of small samples (particularly important at small impact parameter in our work).

The results of our covering factor calculations are given in Table 3 and shown in Figure 4. We report *cumulative* covering factors: each point represents the covering factor for all impact parameters less than the one considered, $f_c(\leq \rho)$, rather than the differential covering factors (i.e., we calculate the covering factors for $\leq \rho$ rather than for $\rho \pm \Delta\rho$). Given the lack of detections, we report one-sided confidence limits (the 90% quantile of the distribution) in Table 3.[6] We emphasize that the results for each impact parameter are not independent, as they include the same measurements as those at smaller impact parameter. Thus the results summarized in Figure 4 do not give information on the *distribution* of covering factors within M31's halo, only on the 90% confidence limits to the covering factor within a given impact parameter. [For interested parties, the limits on the *differential* covering factors are $f_c' \leq 0.162$, 0.188, 0.099 at 90% confidence for 100 kpc-wide bins centered on $\rho = 50$, 150, 250 kpc, respectively.] We also note that our covering factors are only appropriate for regions outside of the H I disk of M31 (i.e., in the CGM). We define

[6] Specifically, we've used Cameron's Equation 3, determining the value of $f_c(\leq \rho)$ (equivalent to that equations's upper bound p_u) for which the integration of the beta distribution between $f_c(\leq \rho)$ and 1 yields a normalized probability of 0.1.

positions associated with the disk as those that would fall on a projected circle of radius $r = 30$ kpc at an inclination angle of $i \approx 78°$ (Braun 1991).

We also show in Figure 4 the results we would obtain if we assume the two H I detections are in fact associated with the CGM of M31, although we stress that this seems highly unlikely (see Appendix). The covering factors derived under this assumption are summarized in Table 4 at impact parameters for which the results are different than those in Table 3. We give three values in Table 4: $f_c(\leq \rho)_{0.1}$, $f_c(\leq \rho)_{0.5}$, $f_c(\leq \rho)_{0.9}$, which correspond to the 10%, 50% (median), and 90% quantiles for the covering factor distributions (again using the incomplete beta generator discussed by Cameron 2011).

We find the covering factor within $R_{\rm vir}$ is $f_c(\leq R_{\rm vir}) \leq 0.051$ (90% confidence limit). Our ability to provide meaningful constraints is dependent on the number of sight lines probed, and thus the limits are not strong in the inner regions where < 10 sight lines were observed (see Figure 4, top). Even though we do not detect H I emission in our survey, one should not be under the impression that there is *no* high column density gas associated with M31's CGM, as Wolfe et al. (2016); Kerp et al. (2016); Westmeier et al. (2005, 2008) have found clumps of high column density gas in the halo (in some cases to $\rho \sim 100$ kpc from the center of M31). However, any such gas must have a very small covering factor at, e.g., $\rho \gtrsim 50$ kpc. Westmeier et al. (2008), for example, find $\sim 95\%$ of the HVCs in their map of a region of the M31 CGM are confined to $\rho \lesssim 50$ kpc (for $M_{\rm HVC} \lesssim 1.3 \times 10^5\ M_\odot$ at 5σ). In our data, gas at column densities $\log N({\rm H\ I}) \gtrsim 17.6$ can be present on scales smaller than the 2 kpc-diameter beam and remain undetected, so long as the total mass is less than our typical sensitivity of $M_{\rm HI} \approx 10^4\ M_\odot$.

Figure 4 also shows an assessment of the covering factor of HVCs about M31 by Richter (2012) (based on the maps of Thilker et al. 2004). The blue curve in Figure 4 shows these results rescaled for our assumed distance and transformed into the cumulative covering factors used here based on Richter's fit. The results beyond $\rho \approx 60$ kpc are an extrapolation of that fit. This fit applies only to the HVC component as defined by Thilker et al. (2004). It excludes the disk of M31. Our new limits are compatible with the HVC covering factors, although the HVCs were observed over an area in which we have few measurements and limited constraints. The HVCs (and "bridge" material) observed about M31 have typical column densities in excess of $\log N({\rm H\ I}) \gtrsim 18$ and masses $M_{\rm HI} \gtrsim 10^5\ M_\odot$, which would be readily detectable by our observations if such material were common in our survey area. While we discuss our results in the general context of the CGM, our definition of CGM is inclusive of "high velocity clouds." Our limits show there is not an abundance of HVCs beyond the mapping limits of those earlier works. A caveat is that our covering factor determinations are limited to $-515 \leq v_{\rm LSR} \leq -170$ km s^{-1}, the lower end set by frequency-switching limits and the upper end set to avoid contamination by Galactic HVCs.

4. COMPARISON WITH RECENT CGM SURVEYS AND SIMULATIONS

4.1. *Comparison with Recent Observations*

The nearest comparison to our measurements from the QSO absorption line literature are those of the COS-Halos survey (Tumlinson et al. 2011, 2013; Prochaska et al. 2017). The original survey targeted AGNs projected within $\rho \sim 150$ kpc of 44 $\sim L^*$galaxies at $z \sim 0.2$, with detection of H I Lyman-series absorption in nearly every case (40/44; see Tumlinson et al. 2013). Such absorption line observations can be sensitive to column densities as low as $\log N({\rm H\ I}) \approx 13$. Most of the H I detections in the original survey had H I column densities that were either orders of magnitude below our detection limits or that were not able to be determined due to the strong saturation of the available Lyman series lines. Follow-up measurements of the Lyman break in some of these these galaxies have recently been completed, providing stronger constraints on their H I column densities (Prochaska et al. 2017). We compare our results with this most recent update.

Figure 5 compares the updated COS-Halos measurements with our measurements in the halo of the Andromeda galaxy. The top panel shows $N({\rm H\ I})$ versus ρ from Prochaska et al. (2017). All of the COS-Halos sight lines are considered, though many of the H I columns (19/44) fall below the lower bounds of this plot. Several of the COS-Halos sight lines have only broad constraints, with lower limits from saturated Lyman series lines or a saturated Lyman break and upper limits from the lack of damping wings on Lyα or Lyβ. Prochaska et al. argue these systems should be treated as having a flat probability distribution in $\log N({\rm H\ I})$ between their lower and upper bounds. We adopt this recommendation, plotting these systems in Figure 5 as extended error brackets (representing the 95% confidence interval) without central values.

There are several caveats to note when comparing our M31 measurements to those of COS-Halos. The COS-Halos sample probes a broad range of galaxy mass/luminosity centered roughly on "L^*." The estimated halo masses for the COS-Halos survey cover the range $11.5 \lesssim \log M_{\rm h}/M_\odot \lesssim 13.7$, with stellar masses $9.6 \lesssim \log M_*/M_\odot \lesssim 11.5$; these

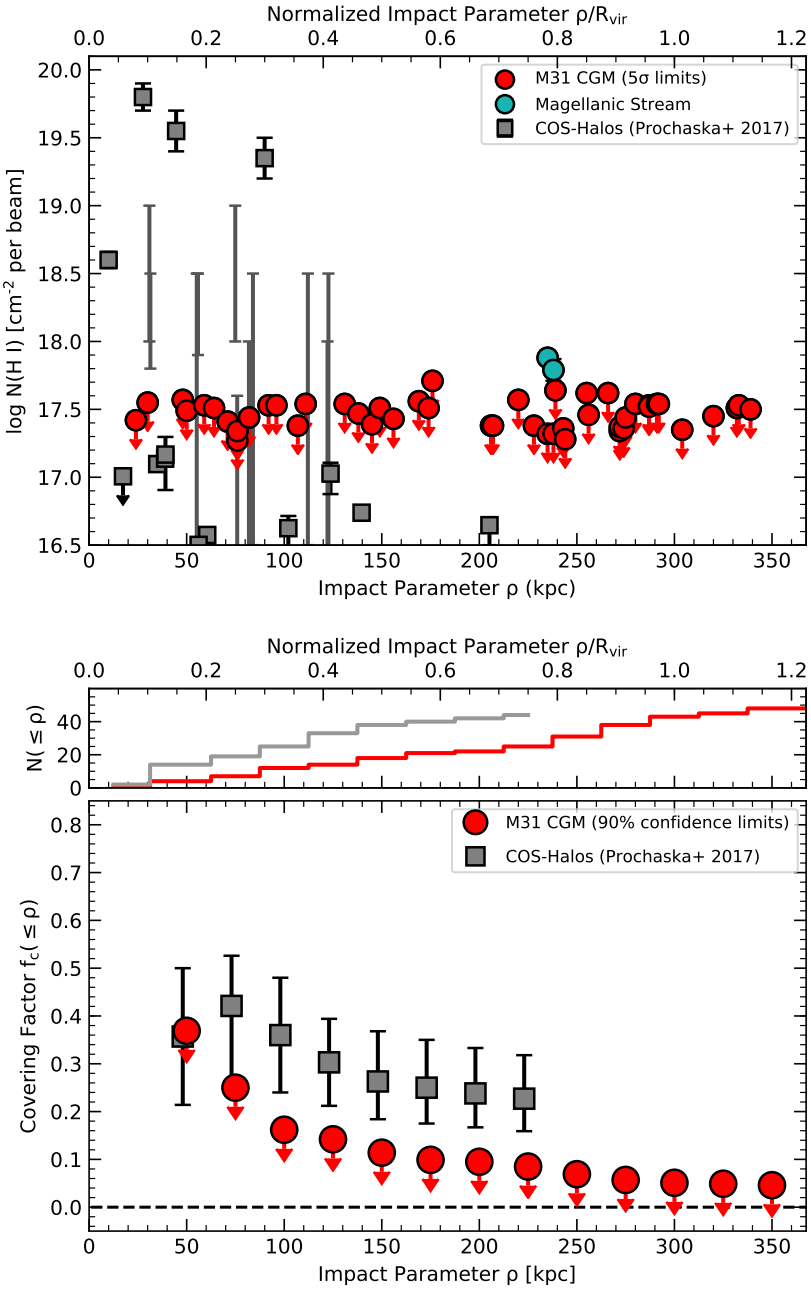

Figure 5. *Top:* The column density limits through the CGM of M31 compared with the results of the absorption-line COS-Halos survey (Prochaska et al. 2017, see also Thom et al. 2012; Tumlinson et al. 2013). The error bars without central values represent sight lines for which Prochaska et al. (2017) bracket the column densities with upper and lower limit, arguing for a flat probability distribution between those 95% confidence limits. Because the COS-Halos results probe galaxies over 2 dex in stellar mass ($9.5 \lesssim \log M_*/M_\odot \lesssim 11.5$), we plot the position of each galaxy according to its normalized impact parameter, $\rho/R_{\rm vir}$ (i.e., according to the impact parameter scale on the top axis) for comparison with the M31 results. Only about half of the COS-Halos systems are seen in this plot, the rest having column densities $\log N({\rm H\ I}) \leq 16.5$. All of the COS-Halos galaxies are at $\rho/R_{\rm vir} \lesssim 0.75$. *Bottom:* Covering factor limits for M31 compared with the covering factor of $\log N({\rm H\ I}) \geq 17.6$ absorption in the ensemble of COS-Halos galaxies. Here we have calculated the cumulative covering factors for the revised COS-Halos survey of H I (Prochaska et al. 2017, see also Thom et al. 2012; Tumlinson et al. 2013). The central value for the COS-Halos results is the median of the output distribution from the Monte Carlo approach described in the text, while the error bars denote the 10% to 90% quantiles. All of the COS-Halos galaxies are at $\rho/R_{\rm vir} \lesssim 0.75$, so we only plot covering factors within that limit. Note that the distribution of sight lines for the COS-Halos sample (grey histogram in the upper panel) is significantly different than that of our Andromeda sample, with the former weighting smaller normalized impact parameters more heavily.

should be compared with the Tamm et al. (2012) estimates for M31 of $\log M_{\rm h}/M_\odot \approx 12.0$ and $\log M_*/M_\odot \approx 11.0$. Thus, we are comparing one galaxy to an ensemble of galaxies with a broad range in masses. Furthermore, due to this broad mass range, the relevant physical scales can vary significantly. We have chosen to present all COS-Halos measurements and results relative to their normalized impact parameter, $\rho/R_{\rm vir}$, which is shown across the top of the figures.[7] For this reason some of the COS-Halos measurements will appear at impact parameters larger than the survey limit of $\rho \lesssim 150$ kpc, as the more massive systems in COS-Halos have virial radii larger than that of M31.

The bottom panel of Figure 5 shows a comparison of the covering factors derived for the Prochaska et al. (2017) results in comparison with ours for M31. The COS-Halos results are based on a Monte Carlo sampling of the full N(H I) distribution over a given (normalized) impact parameter range. We do this to account for the systems with lower and upper bounds on the column density that straddle our detection limit (though we have verified that it gives results indistinguishable from the Cameron 2011 approach if we consider only systems clearly above our detection limit). For each impact parameter considered, we create an N(H I) distribution that is the sum of the probability distribution functions (PDFs) describing each of the COS-Halos measurements. The direct measurements in Prochaska et al. (2017) have reasonably-symmetric errors, and we adopt a normal distribution for each in $\log N$(H I). For the bounded values from Prochaska et al., we follow their recommendation and treat each as having a flat PDF between the limiting columns. For upper limits, we assume a flat PDF between $\log N$(H I) = 10.0 and the quoted upper limits. To calculate the covering factor within a given impact parameter, we create 10,000 realizations of the observations, drawing the same number of H I column densities as sight lines within that range from the full N(H I) distribution. For each realization we calculate the covering factor as the fraction of the mock sight lines with $\log N$(H I) ≥ 17.6. From the full sample of covering factors, we derive the quantiles of the distribution. The bottom panel of Figure 5 shows the results, where the central values give the median of the distribution with error bars representing the [10%, 90%] quantiles (i.e., the 80% confidence interval).

The implied covering factor of gas with $\log N$(H I) ≥ 17.6 for COS-Halos galaxies within $0.5R_{\rm vir}$ is $f_c(\leq 0.5R_{\rm vir}) = 0.26$ [0.18, 0.37] (median and [10%, 90%] quantiles), and it is ≈ 0.36 within $0.33R_{\rm vir}$. (Although they do not normalize to the virial radius, these results are similar to those given by Prochaska et al. (2017), who note the covering factor at $\rho \leq 75$ kpc is $\gtrsim 50\%$ for $\log N$(H I) $\gtrsim 17.2$.) The COS-Halos survey thus shows a striking prevalence of high column density H I absorption systems. A sizeable fraction of the COS-Halos absorption line measurements (at least 8/44) have columns in excess of our detection limit, $\log N$(H I) = 17.6. The mean N(H I) for gas with $\log N$(H I) ≥ 17.6 from COS-Halos is $\log\langle N({\rm H\ I})\rangle_{\geq 17.6} = 19.15$ (with a geometric mean $\langle \log N({\rm H\ I})\rangle_{\geq 17.6} = 18.65$). This gas is detected frequently enough that the mean N(H I) drawn from our construction of the full N(H I) distribution of Prochaska et al. (2017) is $\log\langle N({\rm H\ I})\rangle = 18.51$.

In roughly 30% of the COS-Halos galaxies, gas with $\log\langle N({\rm H\ I})\rangle_{\geq 17.6} = 19.15$ is observed within $0.5R_{\rm vir}$. Any of our observations intercepting gas with this column density would readily detect such gas if it covered 30% of our 2 kpc beams. Thus, if the mean COS-Halos statistics are a fair representation of the structure of N(H I) on small scales – specifically as good reprentations of the fraction of a 2 kpc diameter beam covered by any high column density gas clouds – we should have detected any clouds having high H I columns like those seen in the COS-Halos measurements. Indeed, gas with $\log N$(H I) = 19.15 would need to cover $\leq 2.8\%$ of our beam to avoid detection, some $10\times$ lower than implied by the COS-Halos covering factors.

It is the case that the radial distributions of sight lines in COS-Halos and our sample are weighted differently. The high column density H I absorbers in COS-Halos are at $\rho \lesssim 0.33R_{\rm vir}$ (Figure 5). Even considering only this range in impact parameter, however, our M31 covering factors $f_c(\leq 0.33R_{\rm vir})$ aren't consistent with those in the COS-Halos galaxies. Thus, it is difficult to reconcile the ensemble results from COS-Halos with our measurements of H I in the CGM of the Andromeda galaxy.

The COS-Halos galaxies that show gas at $\log N$(H I) ≥ 17.6 have a mean stellar mass $\langle \log M_*/M_\odot\rangle \approx 10.9$ (full range 10.2 to 11.3), so this high column density gas resides in the halos of galaxies similar to M31. It is perhaps noteworthy that the COS-Halos survey attempted to select against pairs of L^* galaxies (Tumlinson et al. 2013), such as the M31-Milky Way pair. Thus, if M31 were at $z \sim 0.2$, it may not have been been included in the COS-Halos survey. If its Local Group membership plays a role in determining the covering factor, the M31/COS-Halos comparison could be inappropriate (although the halos in the Local Group-like simulations of Nuza et al. 2014 show results similar to those of the single-halo simulations discussed below). However, because the initial selection was done using photometric redshifts, this selection against galaxy pairs was not as clear cut as initially intended (Werk et al. 2012).

[7] The results of our comparison are not fundamentally different if we consider the results with ρ rather than the normalized coordinate.

In general metal absorption lines show higher covering factors about galaxies than our H I 21-cm measurements about M31. Metal lines are found with covering factors $> 60\% - 75\%$ within $\sim 0.5 R_{\rm vir}$ (e.g., Chen et al. 2010; Nielsen et al. 2013; Stocke et al. 2013; Werk et al. 2014; Borthakur et al. 2016). Indeed, LHW15 find covering factors near unity for C II and Si III absorption within $\rho \lesssim 0.5 R_{\rm vir}$, albeit with a very small sample. Preliminary results from Project AMIGA still support a high covering factor in these ions (N. Lehner et al. in prep). The metal lines show higher covering factors in part due to the greater sensitivity of absorption line techniques to low column density gas (e.g., Lyα absorption lines are detectable to $\log N({\rm H\ I}) < 12.5$), but it is also a reflection of the general ionization level of gas in the CGM. A majority of the cool and warm gas ($10^{4-5} \leq T \leq T_{\rm vir}$) in galaxy halos is significantly ionized (Werk et al. 2014; Keeney et al. 2017), including the LLS-like regime that we are probing (Lehner et al. 2013; Fumagalli et al. 2016; Lehner et al. 2016).

The metal ion covering factors about M31 are not that different than those found about COS-Halos and other galaxies. But, depending on the degree of saturation within the detected metals, we should not necessarily expect to see the same covering factor in high H I column density gas. We have compared the LHW15 measurements along the three sight lines with $\rho \lesssim 50$ kpc relative to M31 to the COS-Halos results. All of the COS-Halos with high H I column densities ($\log N({\rm H\ I}) \geq 17.6$) also have significantly higher Si II, Si III, and C II columns than the three inner-halo Andromeda sight lines. These COS-Halos systems have $> 2-3\times$ higher Si III columns than M31 (all are lower limits due to saturation in the COS-Halos sight lines) and $\sim 10\times$ higher Si II column densities. Thus, it appears the COS-Halos sight lines simply probe higher column densities of low-ionization gas, including H I. This is hidden by the comparison of metal ion covering factors because the metal absorption lines are so sensitive and quick to saturate. The metal / H I ratios in M31 appear to be consistent with those found by COS-Halos.

4.2. *Comparison with Recent Simulations*

The covering factors of H I and metal ions are considered in a number of simulation papers (Fumagalli et al. 2011a; Faucher-Giguère & Kereš 2011; Shen et al. 2012; Fernández et al. 2012; Fumagalli et al. 2014; Faucher-Giguère et al. 2015; Suresh et al. 2015; Faucher-Giguère et al. 2016; Gutcke et al. 2016; Liang et al. 2016). The motivation for extracting this quantity from simulations arises in part because this is an observable quantity (Rudie et al. 2012; Prochaska et al. 2013), but also because the covering factor can respond to changes in the accretion rate and feedback intensity in a galaxy and the numerical approaches adopted. For example, the covering factors of LLS absorption can change by factors of > 2 depending on the wind models adopted or presence of AGN activity (e.g., Suresh et al. 2015). Most commonly the predictions are made for $z \sim 2$, not only because the simulations are less expensive to run to these redshifts, but also because there are more measurements of the H I covering factor at high redshift than at $z \sim 0$, which typically requires space-based observations. At the same time, the choice of the limiting H I column for reporting the covering factors varies widely, depending on the focus of the simulations.

With this in mind, we compare our observations of M31 with the recent simulations reported in H17, who investigated the relationship of $z < 1$ LLSs to galaxies; these halos were simulated as part of the FIRE project (Hopkins et al. 2014). Figure 6 compares our results with an ensemble of cosmological zoom simulations from H17, shown with the green curve and shaded regions. The analysis of H17 produce simulated column density distributions for their ensemble of galaxies, which they found to be consistent with the cosmological incidence rates of low-redshift ($0 \leq z \leq 1.0$) LLSs at $\log N({\rm H\ I}) \geq 17.5$ and $\log N({\rm H\ I}) \geq 17.2$ (Ribaudo et al. 2011). These simulations however have difficulties matching the observed metallicity distribution of low-z LLSs (Lehner et al. 2013; Wotta et al. 2016). The results summarized in Figure 6 are from the four halos studied in H17 whose final ($z = 0$) masses are $11.8 \leq \log M_{\rm h}/M_{\odot} \leq 12.1$ (simulations m11.9a, m12i, m12q, m12v of H17). The simulated halos have been projected into a 512^3 grid spanning $2.4 \times R_{\rm vir}$ (with cell sizes ~ 1.0–1.2 kpc) for each simulation. We derived cumulative covering factors for $\log N({\rm H\ I}) \geq 17.6$ using normalized impact parameters $\rho/R_{\rm vir}$ as we did in the COS-Halos comparison. We consider each of the simulated galaxies from three orthogonal perspectives and use 11 snapshots per simulation over the redshift range $0 \leq z \leq 0.25$. Thus there are 132 total models that go into calculating $f_c(\leq \rho)$ and its quantiles for each impact parameter bin (which are sampled in steps of $0.1\,\rho/R_{\rm vir}$).

The thick curve in Figure 6 shows the median of the H17 results, the darkest shading shows the interquartile range (from the 25% to 75% quantiles), and the lightest shading shows the 5% to 95% quantile range. The median results show that the covering factor from these simulations of high column density gas around galaxies in the mass range analyzed is generally relatively small, with simulated median covering factors $f_c(\leq 0.5 R_{\rm vir}) = 0.037$ and $f_c(\leq R_{\rm vir}) = 0.011$. These compare with our upper limits of < 0.11 and < 0.051 at 90% confidence for the same two impact parameters; they are significantly lower than the results from COS-Halos at these same impact parameters. We point out that the simulations display significant variations in the covering factors. The variations are a result of both strong time-

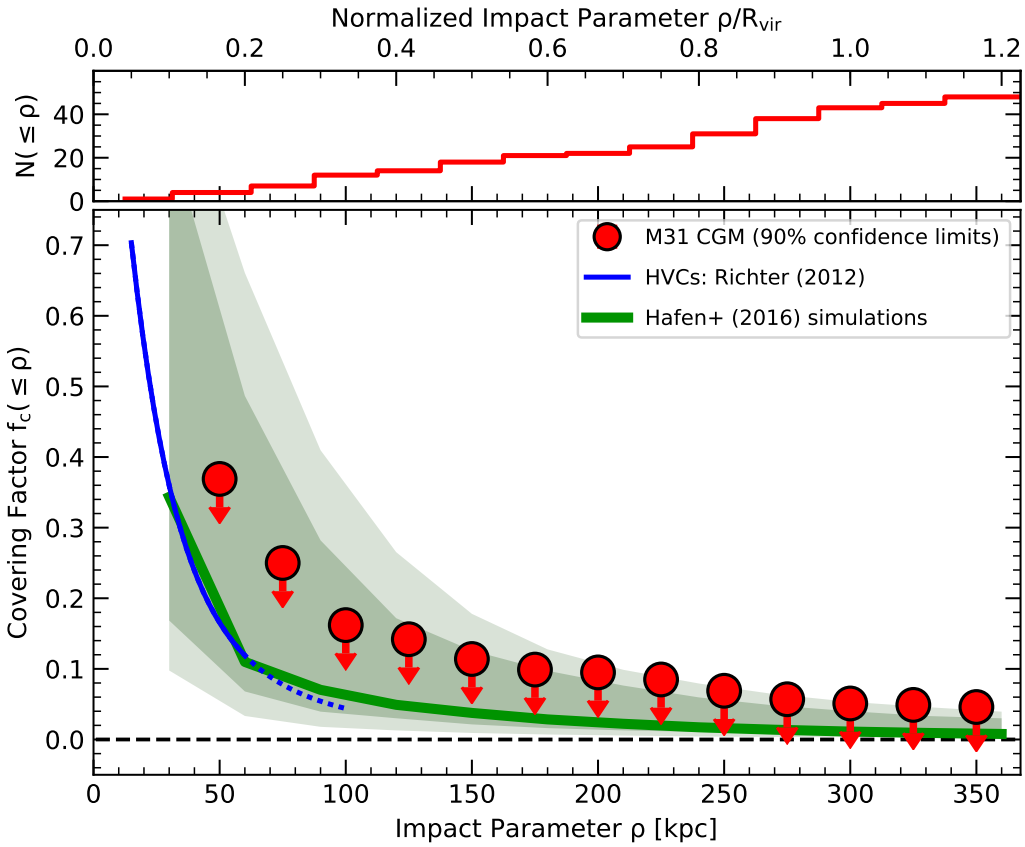

Figure 6. The cumulative covering factors for M31 compared with simulation results. The green line represents the median cumulative covering factor from the $11.8 \leq \log M_{\rm h}/M_{\odot} \leq 12.1$ simulations of Hafen et al. (H17), while the dark and light green shading shows the [25%, 75%] (interquartile) and [5%, 95%] ranges from these models. The median simulation result has a covering factor $f_c(\leq R_{\rm vir}) = 0.011$. Our limits on the covering factor from M31 are consistent with expectations from these simulations.

dependence related to wind and accretion activity (in the case of the H17) as well as variations between different galaxy halos (Faucher-Giguère et al. 2015; Muratov et al. 2015, H17).

The highest covering factors in the simulations arise in the inner regions of the galaxies. We do not sample $\rho \lesssim 50$ kpc well with our 21-cm observations due to our focus on directions with known UV-bright AGN (we have only 4 directions in this regime). In the inner regions (within $\rho \approx 0.33 R_{\rm vir} \approx 100$ kpc) the FIRE simulations from H17 seem to be in good agreement with the covering factors derived for M31's HVC population (Richter 2012).

Other simulations find results similar to those of H17. For example, Gutcke et al. (2016) find $f_c \approx 0\% - 10\%$ for $\log N({\rm H\,I}) \geq 17.2$ in simulations of M31-like mass galaxies at $z \sim 0$, where the range represents the variations seen in simulations of different galaxies. Fernández et al. (2012) presented a high-resolution simulation of a single M31-like halo, and they found H I covering factors reasonably consistent with the Richter (2012) distribution for $\log N({\rm H\,I}) \geq 17.7$. Nuza et al. (2014) considered a Local Group-like configuration of halos; they find very high covering factors in the inner regions of those two halos, and results that are generally consistent with our observations. Our measurements in M31 are consistent with the median set of simulations in all of these cases, showing a quite low covering factor of optically-thick H I when assessed within $R_{\rm vir}$.

5. DISCUSSION

In this work, we have investigated the frequency of optically-thick gas with $\log N({\rm H\,I}) \geq 17.6$ about the local L^* galaxy M31. On the basis of GBT searches for 21-cm emission with a 2 kpc beam, we find a minimal covering factor of such gas in the halo of the Andromeda galaxy. We derive a covering factor within the virial radius of $f_c(\leq R_{\rm vir}) < 0.051$. Our limits on the cumulative covering factor are not particularly strong in the inner halo (esp., $\rho \lesssim 0.25 R_{\rm vir}$), where we have few pointings. Complementary information exists from the previous HVC results within $\rho \lesssim 0.2 R_{\rm vir}$ (Thilker et al. 2004; Richter 2012).

There is some discrepancy in our assessment with previous work on the H I environment of the M31/M33 system. As noted earlier, the initial maps by Braun & Thilker (2004) seem to show more wide-spread emission than is present (Lockman et al. 2012; Wolfe et al. 2013, 2016).[8] More recently, Kerp et al. (2016) have emphasized the potential for blending of high-velocity M31 structures with the Milky Way's 21-cm emission. They attempted to decompose the complicated region around M31 with guidance from continuities in the "difference second moment map," arguing that several very large H I complexes within $\rho \sim 80$ kpc are associated with M31. These complexes span tens of kpc at the distance of M31. We would not have included them as detections in our survey because they lie outside of our velocity range. The Kerp et al. structures are at $-150 \lesssim v_{\rm LSR} \lesssim -100$ km s^{-1} (within ≈ 200 km s^{-1} of M31's systemic velocity), whereas our survey is restricted to $-515 \leq v_{\rm LSR} \leq -170$ km s^{-1} in order to avoid contamination by Galactic HVC emission. Furthermore, none of our pointings directly intersect the clouds they identify, a by-product of our low sampling density at small impact parameters. Assuming all of the clouds Kerp et al. identify are indeed associated with M31, their Figure 7 implies covering factors just consistent with our limits. For example, their map implies $f_c(\leq 0.33R_{\rm vir}) \approx 0.2$ (ignoring emission within 25 kpc in order to exclude the disk), which compares with our limit $f_c(\leq 0.33R_{\rm vir}) \leq 0.16$ at 90% confidence. This covering factor estimate is dominated by the two large structures that they identify on opposite sides of the galaxy (their clouds *a* and *b*). It is a bit disconcerting that the two structures, separated by many tens of kpc, both lie at the extreme positive velocities expected for circumgalactic material about M31 (both with $v_{\rm LSR} \approx -115$ km s^{-1}). It is not clear why two structures separated by more than the diameter of M31's disk should have the exact same extreme velocity. The covering factors implied by the Kerp et al. (2016) are $\sim 2\times$ higher than those of Richter (2012) at the same impact parameters. This discrepancy is wholly connected to the issues of blending with Milky Way HVC gas at $v_{\rm LSR} \gtrsim -170$ km s^{-1}. While Kerp et al. attempt to solve it through a unique approach, it is difficult to verify their results with other means.

In general our limits to the H I covering factor are quite consistent with the low values expected from cosmological zoom simulations of individual galaxies at $z \approx 0$ (Gutcke et al. 2016, H17). With no detections, we do not have a valid characterization of the shape of the f_c distribution about M31, although the work by Richter (2012) provides a fit to the HVC covering factor within ~ 60 kpc. Some of the simulated galaxies show higher f_c than is observed in M31, as captured in the simulations ranges shown in Figure 6. This is a result of the halo-to-halo variations as well as the significant temporal variations within a single halo (Rahmati et al. 2015; Faucher-Giguère et al. 2015, H17). Thus, while the covering fraction of optically-thick gas about M31 is not in conflict with the simulations, it is a single sample from a specific time. It may be drawn from a broad distribution like those seen in the simulations.

As discussed in §4.1, our results appear discrepant from the COS-Halos galaxies (Tumlinson et al. 2013; Prochaska et al. 2017). There are very few other works that put strong constraints on the covering factor of optically-thick gas about low-redshift galaxies. There could be a multitude of physical reasons for the difference between M31 and COS-Halos: 1) M31 could have experienced significant evolution in the last 2.5 Gyr, the time since the typical redshift of the COS-Halos galaxies; 2) "green valley" galaxies with star formation rates like M31, which are not well sampled by COS-Halos, may have distinct CGM properties; 3) the presence of M31 in a group with another massive spiral, which would have been (mildly) selected against in the COS-Halos sample, may affect its CGM. However, it's unlikely we could distinguish these effects from simple stochastic variations for a single galaxy.

The environment of M31 could plausibly play a role in shaping its CGM. Burchett et al. (2016) found a smaller detection rate (covering factor) of C IV for galaxies in high density environments (assessed over $\rho \approx 1.5$ Mpc). They do not find a corresponding difference in H I covering factor, but their dynamic range in N(H I) is small due to saturation of Lyα (they cannot probe columns higher than $\log N$(H I) ~ 14.5). However, the Local Group would not be included in their high density category, as only 2-3 galaxies would make their luminosity cut ($M_r < -19$ mag) for identifying galaxies in their density counting scheme. We note that Nuza et al. (2014) have presented simulations of a Local Group-like pair of halos, both of which show high covering factors. They find near unity (differential) covering factors for gas at $\log N$(H I) $\gtrsim 17.85$ to 30-50 kpc in their two halos. However, this is based on only one pair of halos seen at a single time, so we cannot yet draw strong conclusions based on these simulations.

In general higher covering fractions are found from metal absorption line searches. Several studies of strong Mg II absorption (typically $W_r \gtrsim 0.3$ mÅ) have found quite high covering factors (e.g., > 0.6) within $\sim R_{\rm vir}$ (Chen et al. 2010; Nielsen et al. 2013), even for relatively massive galaxies like M31. Some of this difference has to do with the broad range of H I column densities probed by Mg II absorption, which can trace gas over nearly 5 orders of magnitude

[8] These works generally show a very low detection rate in their searches, consistent with our low covering factor determinations. However, because these works studied areas specifically to address previous potential detections of H I by Braun & Thilker (2004), their observations are not suitable for general covering factor calculations, as they may be biased in favor of H I detections. Nonetheless, these efforts all support a small covering factor on small scales, even in directions suspected originally to have H I emission.

in N(H I) (gas with $\log N$(Mg II) ~ 13 – $W_r(2796) \sim 0.3$ mÅ – can probe solar metallicity gas with $\log N$(H I) ~ 16 or damped Lyα systems with $< 1/300$ of the solar metallicity; Wotta et al. 2016).

We note that Rao et al. (2013) searched for the signature of Mg II and other low-ion absorption from the halo of M31 using low-resolution COS spectra. They probed impact parameters $13 \lesssim \rho \lesssim 112$ kpc with 10 AGNs, finding absorption in four sight lines, all of which reside at $\rho \lesssim 40$ kpc and within the $\log N$(H I) ~ 18.3 contours of the 21-cm measurements. Their observations, sensitive to $W_r(2796) \sim 0.3 - 0.5$ Å, targeted AGNs projected along M31's major axis. The lack of absorption in their four targets at $40 \lesssim \rho \lesssim 112$ kpc is perhaps not surprising given the small number of sight lines and the low covering factor of high column density gas we find (their low-resolution observations have sensitivity to only $W_r(2796) \sim 300$ mÅ, whereas Project AMIGA's sensitivity is ~ 20 mÅ).

Roughly half of the sight lines observed in this work have been observed by *HST*/COS at intermediate resolution (G130M+G160M) as part of Project AMIGA. These observations, a subset of which were published by LHW15, are sensitive to relatively weak metal line absorption, notably in transitions from the ions C II, C IV, Si II, Si III, Si IV. The preliminary data from this program suggest a quite high metal line covering factor. One of the initial goals for Project AMIGA GBT was to provide an H I reference for potential metallicity estimates, since Lyα absorption from the Andromeda galaxy is swamped by the Galactic absorption trough. Unfortunately, with only upper limits on N(H I) coupled with potential beam-dilution effects, we cannot provide a hydrogen reference for the metallicity determination. Without the hydrogen reference, determining the metallicities along these sight lines will not be possible (on this point we disagree with the recent work of Koch et al. 2015).

Better constraining the covering factor in the inner regions of M31's CGM may be readily accomplished by simply observing more sight lines (and more GBT observations are forthcoming). The H I maps of Thilker et al. (2004) as analyzed by Richter (2012) provide some guidance in this inner region, albeit at worse mass sensitivity than the current observations and only at $\rho \lesssim 50$ kpc. Pushing below our current H I column density limits, which are in the range of $\log N$(H I) ~ 17.4 to 17.6 at 5σ, is in principle possible. However, in many of the cases presented here the limiting factor in the H I sensitivity is the quality of the spectral baselines. The GBT baselines are already among the best available, but we are working near the limit for the current instrumentation.

6. SUMMARY

We have used the Green Bank Observatory's 100-m Robert C. Byrd Green Bank Telescope to search for 21-cm emission from the CGM of our neighbor M31. We detect no H I emission, with column density limits that overlap studies of QSO absorption line experiments (notably the LLSs). Our principal conclusions are as follows.

1. We constrain the covering factor of optically-thick H I with $\log N$(H I) $\gtrsim 17.6$ about M31 to be $f_c(\leq R_{\rm vir}) < 0.051$ (90% confidence).

2. Our covering factor limits for these high H I column densities are much lower than those found for metal lines about L^* galaxies, including M31 (LHW15).

3. The covering factors derived here are also discrepant from recent measurements by the COS-Halos project at the same H I column densities (Prochaska et al. 2017). The origin of this difference is not clear. It may be related to characteristics of M31 that are not represented in the COS-Halos sample, although the difference could also be consistent with stochastic variations in M31's CGM with time.

4. The covering factors of optically-thick H I about M31 are consistent those found in recent cosmological zoom simulations.

Part of this manuscript was written at the 2016 Arthur M. Wolfe Symposium in Astrophysics hosted by IMPS of UC Santa Cruz Department of Astronomy. We thank the Esalen Institute for its great setting and wonderful hospitality during that retreat. Support for HST Program number 14268 was provided by NASA through a grant from the Space Telescope Science Institute, which is operated by the Association of Universities for Research in Astronomy, Incorporated, under NASA contract NAS5-26555. Some of this work was supported by NSF grants AST-1212012 and AST-1517353 to Notre Dame and JHU. DJP recognizes partial support from NSF CAREER grant AST-1149491. Contributions by ZH and CAFG were additionally supported through NSF grants AST-1412836 and AST-1517491 and through NASA grant NNX15AB22G. This research made use of Astropy, a community-developed core Python package for Astronomy (Astropy Collaboration et al. 2013), and the matplotlib plotting package (Hunter 2007).

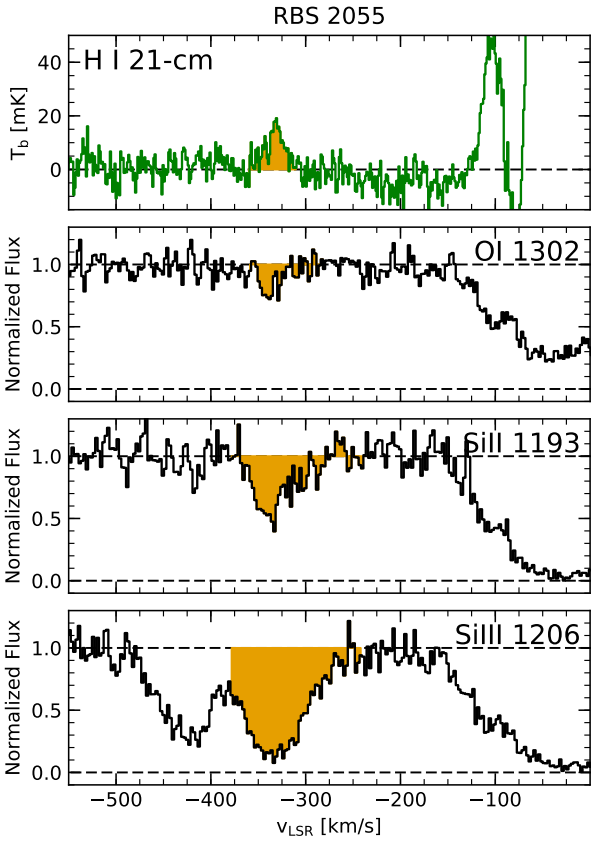

Figure A1. COS absorption line spectra of the sight line to RBS 2055 compared with the GBT H I emission along this sight line (top). The metal absorption lines are O I λ1302, Si II λ1193, and Si III λ1206 (top to bottom). The shaded areas represent the region over which the column densities were determined (the GBT columns were determined via a Gaussian fit, the COS absorption columns via direct integration). The Si III absorption contains unresolved saturation, giving only a lower limit to the column density (see LHW15). In addition, the lesser saturation of the gas at $v_{\rm LSR} \gtrsim -310$ km s^{-1} relative to the principal component centered at $v_{\rm LSR} \approx -335$ km s^{-1} causes the central velocity of the much stronger Si III line to appear at higher velocities relative to the other transitions. These measurements together provide a measure of the metallicity, [O/H] $= -0.95 \pm 0.12$.

Facility: GBT

Software: Astropy (Astropy Collaboration et al. 2013),GBTIDL (Marganian et al. 2006), Matplotlib (Hunter 2007)

APPENDIX

A. METAL LINES TOWARD RBS 2055

The sight lines with detected H I emission – toward RBS 2055 and RBS 2061 – both lie close to the MS, and the velocity of this emission is similar to expectations for the MS in these directions. Figure A1 shows a few transitions from our Project AMIGA HST/COS spectra of the sight line to RBS 2055 (N. Lehner et al., in prep.). We detect absorption from a wide range of ions, including C II, O I, Si II, Si III, and Si IV. These are centered at $v_{\rm LSR} \approx -335$ km s^{-1}, very slightly offset from the centroid of our apparent H I emission in this direction, but well within the COS wavelength calibration uncertainties. The detection of O I is noteworthy, in that it implies a high column density of H I, in agreement with our direct 21-cm observations, and because O I is not detected along any of the other sight lines at large impact parameters in our Project AMIGA data outside of the region projected near to the MS.

The detection of O I is also significant because the ionization fractions of O I and H I are coupled by a strong charge exchange reaction (Chambaud et al. 1980; Stancil et al. 1999, e.g.,). Thus ionization corrections that might apply in

transforming measures of $N(\mathrm{O\ I})/N(\mathrm{H\ I})$ into the O/H abundance ratio are generally very small (e.g., Fox et al. 2013). We measure an O I column density in this gas $\log N(\mathrm{O\ I}) = 13.62 \pm 0.11$. Comparing this directly to our H I column density measurements from Table 2 (assuming ionization corrections are very small) yields an estimated abundance $[\mathrm{O/H}] = -0.95 \pm 0.12$ (statistical errors only). This value is in good agreement with several measurements made along the main body of the MS by Fox and collaborators. Fox et al. (2010, 2013) have derived $[\mathrm{O/H}] = -1.0$ to -1.2 in several regions along the MS. These include a measurement along the sight line to NGC 7469, only $\sim 21°$ from RBS 2055, which shows $[\mathrm{O/H}] = -1.00 \pm 0.05$ (statistical errors only) for a column density of $\log N(\mathrm{H\ I}) = 18.62 \pm 0.03$ from GBT+Effelsberg observations (Fox et al. 2013). These measurements were made in the same way as our abundance estimate: comparing metal lines (O I in most cases) with ground-based H I 21-cm measurements. Thus, our metallicities should be directly comparable to those of Fox et al..

Given the location of these sight lines close to the great circle on which the MS lies, as well as the overall agreement in the expected velocities and metallicities, we conclude that the emission detected toward RBS 2055 and the nearby RBS 2061 arises in the MS. There are sight lines in our sample near to the MS that lack emission at these velocities. However, this is not unexpected, as the MS is quite patchy in this direction (this region is referred to as the "tip" of the MS by Nidever et al. 2010). We also note that at velocities outside of $-350 \lesssim v_{\mathrm{LSR}} \lesssim -300$ km s^{-1}, the RBS 2055 and RBS 2061 sight lines show no other emission. This is in contrast to the COS data toward RBS 2055, which show well-detected absorption at $v_{\mathrm{LSR}} \sim -420$ km s^{-1} in ions such as Si II, Si III, and C IV, presumably from the CGM of M31 (Figure A1 and N. Lehner et al., 2017, in prep.).

Having concluded that the gas at $v_{\mathrm{LSR}} \approx -330$ km s^{-1} in this direction probes the MS, our absorption line data provide measures of the physical conditions in the MS gas. Our observations include Si II, Si III, and Si IV. The summed column density of these ions is $\log N(\mathrm{Si}) \geq 13.73 \pm 0.02$. These ions together probe the low- to moderate-ionization gas in the MS, including photoionized gas and collisionally-ionized gas at $T \lesssim 70,000$ K. O I is a tracer of the neutral gas content. Thus, the ratio of O I to the total Si column provides a measure of the ionization fraction of the gas (see Lehner et al. 2015). The H I ionization fraction derived for the cool/warm gas along this sightline is $x(\mathrm{H^0}) \equiv N(\mathrm{H^0})/N(\mathrm{H}) > 0.97$, implying a total column density of $\log N(\mathrm{H\ I + H\ II}) > 19.6$, similar to that found in a much larger sample of MS sight lines by Fox et al. (2014). If one excludes the gas associated with Si IV, imagining it resides in much different physical conditions than the lower ionization gas, the result is not much changed ($x(\mathrm{H^0}) > 0.96$), since Si IV is only $\sim 25\%$ of the total column.

REFERENCES

Anderson, M. E., Bregman, J. N., & Dai, X. 2013, ApJ, 762, 106

Anglés-Alcázar, D., Faucher-Giguère, C.-A., Kereš, D., et al. 2016, ArXiv e-prints, arXiv:1610.08523

Astropy Collaboration, Robitaille, T. P., Tollerud, E. J., et al. 2013, A&A, 558, A33

Blitz, L., & Robishaw, T. 2000, ApJ, 541, 675

Boothroyd, A. I., Blagrave, K., Lockman, F. J., et al. 2011, A&A, 536, A81

Borthakur, S., Heckman, T., Tumlinson, J., et al. 2016, ApJ, 833, 259

Braun, R. 1991, ApJ, 372, 54

Braun, R., & Thilker, D. A. 2004, A&A, 417, 421

Brown, T. M., Smith, E., Ferguson, H. C., et al. 2006, ApJ, 652, 323

Burchett, J. N., Tripp, T. M., Bordoloi, R., et al. 2016, ApJ, 832, 124

Cameron, E. 2011, PASA, 28, 128

Chambaud, G., Levy, B., Millie, P., et al. 1980, Journal of Physics B Atomic Molecular Physics, 13, 4205

Chen, H.-W., Helsby, J. E., Gauthier, J.-R., et al. 2010, ApJ, 714, 1521

de Vaucouleurs, G., de Vaucouleurs, A., Corwin, Jr., H. G., et al. 1991, Third Reference Catalogue of Bright Galaxies. Volume I: Explanations and references. Volume II: Data for galaxies between 0^h and 12^h. Volume III: Data for galaxies between 12^h and 24^h.

Dickey, J. M., & Lockman, F. J. 1990, ARA&A, 28, 215

Emerick, A., Mac Low, M.-M., Grcevich, J., & Gatto, A. 2016, ApJ, 826, 148

Fardal, M. A., Babul, A., Guhathakurta, P., Gilbert, K. M., & Dodge, C. 2008, ApJL, 682, L33

Faucher-Giguère, C.-A., Feldmann, R., Quataert, E., et al. 2016, MNRAS, 461, L32

Faucher-Giguère, C.-A., Hopkins, P. F., Kereš, D., et al. 2015, MNRAS, 449, 987

Faucher-Giguère, C.-A., & Kereš, D. 2011, MNRAS, 412, L118

Fernández, X., Joung, M. R., & Putman, M. E. 2012, ApJ, 749, 181

Ford, A. B., Davé, R., Oppenheimer, B. D., et al. 2014, MNRAS, 444, 1260

Fox, A. J., Richter, P., Wakker, B. P., et al. 2013, ApJ, 772, 110

Fox, A. J., Savage, B. D., & Wakker, B. P. 2006, ApJS, 165, 229

Fox, A. J., Wakker, B. P., Smoker, J. V., et al. 2010, ApJ, 718, 1046

Fox, A. J., Wakker, B. P., Barger, K. A., et al. 2014, ApJ, 787, 147

Fumagalli, M., Fossati, M., Hau, G. K. T., et al. 2014, MNRAS, 445, 4335

Fumagalli, M., O'Meara, J. M., & Prochaska, J. X. 2011a, Science, 334, 1245

—. 2016, MNRAS, 455, 4100

Fumagalli, M., Prochaska, J. X., Kasen, D., et al. 2011b, MNRAS, 418, 1796

Grcevich, J., & Putman, M. E. 2009, ApJ, 696, 385

Gutcke, T. A., Stinson, G. S., Macciò, A. V., Wang, L., & Dutton, A. A. 2016, MNRAS, arXiv:1602.06956
Hafen, Z., Faucher-Giguere, C.-A., Angles-Alcazar, D., et al. 2017, ArXiv e-prints, arXiv:1608.05712
Heckman, T. M., Armus, L., & Miley, G. K. 1990, ApJS, 74, 833
Hopkins, P. F., Keres, D., Onorbe, J., et al. 2014, Monthly Notices of the Royal Astronomical Society, 445, 581
Hunter, J. D. 2007, Computing In Science & Engineering, 9, 90
Huo, Z.-Y., Liu, X.-W., Xiang, M.-S., et al. 2013, AJ, 145, 159
Joung, M. R., Putman, M. E., Bryan, G. L., Fernández, X., & Peek, J. E. G. 2012, ApJ, 759, 137
Kacprzak, G. G., Cooke, J., Churchill, C. W., Ryan-Weber, E. V., & Nielsen, N. M. 2013, ApJL, 777, L11
Kacprzak, G. G., Martin, C. L., Bouché, N., et al. 2014, ApJL, 792, L12
Keeney, B. A., Stocke, J. T., Danforth, C. W., et al. 2017, ApJS, 230, 6
Kereš, D., Katz, N., Weinberg, D. H., & Davé, R. 2005, MNRAS, 363, 2
Kerp, J., Kalberla, P. M. W., Ben Bekhti, N., et al. 2016, A&A, 589, A120
Koch, A., Danforth, C. W., Rich, R. M., Ibata, R., & Keeney, B. A. 2015, ApJ, 807, 153
Lehner, N., & Howk, J. C. 2011, Science, 334, 955
Lehner, N., Howk, J. C., Thom, C., et al. 2012, MNRAS, 424, 2896
Lehner, N., Howk, J. C., & Wakker, B. P. 2015, ApJ, 804, 79 (LHW15)
Lehner, N., O'Meara, J. M., Howk, J. C., Prochaska, J. X., & Fumagalli, M. 2016, The Astrophysical Journal, 833, 283
Lehner, N., Howk, J. C., Tripp, T. M., et al. 2013, ApJ, 770, 138
Liang, C. J., Kravtsov, A. V., & Agertz, O. 2016, MNRAS, 458, 1164
Lockman, F. J., Free, N. L., & Shields, J. C. 2012, AJ, 144, 52
Marganian, P., Garwood, R. W., Braatz, J. A., Radziwill, N. M., & Maddalena, R. J. 2006, in Astronomical Society of the Pacific Conference Series, Vol. 351, Astronomical Data Analysis Software and Systems XV, ed. C. Gabriel, C. Arviset, D. Ponz, & S. Enrique, 512
McConnachie, A. W. 2012, AJ, 144, 4
Muratov, A. L., Kereš, D., Faucher-Giguère, C.-A., et al. 2015, MNRAS, 454, 2691
—. 2017, MNRAS, 468, 4170
Nidever, D. L., Majewski, S. R., Burton, W. B., & Nigra, L. 2010, The Astrophysical Journal, 723, 1618
Nidever, D. L., Majewski, S. R., & Butler Burton, W. 2008, ApJ, 679, 432
Nielsen, N. M., Churchill, C. W., & Kacprzak, G. G. 2013, ApJ, 776, 115
Nuza, S. E., Parisi, F., Scannapieco, C., et al. 2014, MNRAS, 441, 2593
Oppenheimer, B. D., Davé, R., Kereš, D., et al. 2010, MNRAS, 406, 2325
Peeples, M. S., Werk, J. K., Tumlinson, J., et al. 2014, ApJ, 786, 54
Prestage, R. M., Constantikes, K. T., Hunter, T. R., et al. 2009, IEEE Proceedings, 97, 1382
Prochaska, J. X., Hennawi, J. F., & Simcoe, R. A. 2013, ApJL, 762, L19
Prochaska, J. X., Weiner, B., Chen, H.-W., Mulchaey, J., & Cooksey, K. 2011, ApJ, 740, 91
Prochaska, J. X., Werk, J. K., Worseck, G., et al. 2017, ApJ, 837, 169
Putman, M. E., Peek, J. E. G., Muratov, A., et al. 2009, ApJ, 703, 1486
Rahmati, A., Schaye, J., Bower, R. G., et al. 2015, MNRAS, 452, 2034
Rao, S. M., Sardane, G., Turnshek, D. A., et al. 2013, MNRAS, 432, 866
Ribaudo, J., Lehner, N., & Howk, J. C. 2011, ApJ, 736, 42
Richter, P. 2012, ApJ, 750, 165
Riess, A. G., Fliri, J., & Valls-Gabaud, D. 2012, ApJ, 745, 156
Rubin, K. H. R., Prochaska, J. X., Koo, D. C., et al. 2014, ApJ, 794, 156
Rudie, G. C., Steidel, C. C., Trainor, R. F., et al. 2012, Astrophys. J., 750, 67
Rupke, D. S., Veilleux, S., & Sanders, D. B. 2005, ApJS, 160, 87
Schaye, J. 2001, ApJ, 559, 507
Schwartz, C. M., & Martin, C. L. 2004, ApJ, 610, 201
Shen, S., Madau, P., Aguirre, A., et al. 2012, ApJ, 760, 50
Shen, S., Madau, P., Guedes, J., et al. 2013, ApJ, 765, 89
Spekkens, K., Urbancic, N., Mason, B. S., Willman, B., & Aguirre, J. E. 2014, ApJL, 795, L5
Spitzer, L. 1978, Physical processes in the interstellar medium, doi:10.1002/9783527617722
Stancil, P. C., Schultz, D. R., Kimura, M., et al. 1999, A&AS, 140, 225
Steidel, C. C. 1990, ApJS, 74, 37
Stocke, J. T., Keeney, B. A., Danforth, C. W., et al. 2013, ApJ, 763, 148
Suresh, J., Bird, S., Vogelsberger, M., et al. 2015, MNRAS, 448, 895
Tamm, A., Tempel, E., Tenjes, P., Tihhonova, O., & Tuvikene, T. 2012, A&A, 546, A4
Thilker, D. A., Braun, R., Walterbos, R. A. M., et al. 2004, ApJL, 601, L39
Thom, C., Tumlinson, J., Werk, J. K., et al. 2012, ApJL, 758, L41
Tripp, T. M., Meiring, J. D., Prochaska, J. X., et al. 2011, Science, 334, 952
Tumlinson, J., Thom, C., Werk, J. K., et al. 2011, Science, 334, 948
—. 2013, ApJ, 777, 59
Tytler, D. 1982, Nature, 298, 427
van de Voort, F., Schaye, J., Altay, G., & Theuns, T. 2012, MNRAS, 421, 2809
van de Voort, F., Schaye, J., Booth, C. M., Haas, M. R., & Dalla Vecchia, C. 2011, MNRAS, 414, 2458
Voit, G. M., Bryan, G. L., O'Shea, B. W., & Donahue, M. 2015, ApJL, 808, L30
Wakker, B. P., & Savage, B. D. 2009, ApJS, 182, 378
Weiner, B. J., Coil, A. L., Prochaska, J. X., et al. 2009, ApJ, 692, 187
Werk, J. K., Prochaska, J. X., Thom, C., et al. 2012, ApJS, 198, 3
Werk, J. K., Prochaska, J. X., Tumlinson, J., et al. 2014, ApJ, 792, 8
Westmeier, T., Braun, R., & Thilker, D. 2005, A&A, 436, 101
Westmeier, T., Brüns, C., & Kerp, J. 2008, MNRAS, 390, 1691
Wolfe, S. A., Lockman, F. J., & Pisano, D. J. 2016, ApJ, 816, 81
Wolfe, S. A., Pisano, D. J., Lockman, F. J., McGaugh, S. S., & Shaya, E. J. 2013, Nature, 497, 224
Wotta, C. B., Lehner, N., Howk, J. C., O'Meara, J. M., & Prochaska, J. X. 2016, ApJ, 831, 95

Table 1. GBT Targets near M31

QSO name	RA (J2000)	Dec (J2000)	$\Delta\theta^{a}$ (°)	ρ^{b} (kpc)	$\rho/R_{vir}{}^{c}$	$\sigma_{b}{}^{d}$ (mK)	$\log N(\mathrm{H\,I})^{e}$ (5σ sens.)
RXJ0048.3+3941	00 : 48 : 19	+39 : 41 : 11.0	1.9	24	0.08	2.8	17.43
HS0033+4300	00 : 36 : 23	+43 : 16 : 40.2	2.3	30	0.10	10.1	17.55
HS0058+4213	01 : 01 : 31	+42 : 29 : 35.6	3.7	48	0.16	10.4	17.56
RXSJ0043.6+372521	00 : 43 : 42	+37 : 25 : 19.0	3.9	50	0.17	9.2	17.50
ZW535.012	00 : 36 : 20	+45 : 39 : 53.2	4.5	59	0.20	9.6	17.52
Q0030+3700	00 : 30 : 17	+37 : 00 : 54.0	4.9	64	0.21	9.4	17.51
BLANK	01 : 08 : 27	+38 : 58 : 32.0	5.4	71	0.24	7.4	17.41
MS0108.4+3859	01 : 11 : 16	+39 : 15 : 00.0	5.8	76	0.25	1.9	17.27
RXSJ005050.6+353645	00 : 50 : 50	+35 : 36 : 43.0	5.9	76	0.26	6.3	17.34
2E0111.0+3851	01 : 13 : 54	+39 : 07 : 44.0	6.3	82	0.28	7.9	17.44
IRAS00040+4325	00 : 06 : 36	+43 : 42 : 29.0	7.1	92	0.31	9.7	17.53
RXSJ011848.2+383626	01 : 18 : 49	+38 : 36 : 19.0	7.4	96	0.32	9.8	17.53
RXJ0117.7+3637	01 : 17 : 45	+36 : 37 : 14.9	8.2	107	0.36	6.8	17.37
SDSSJ001847.44+341209.5	00 : 18 : 47	+34 : 12 : 09.6	8.5	111	0.37	9.9	17.54
MRK352	00 : 59 : 53	+31 : 49 : 37.1	10.0	131	0.44	9.9	17.54
RXJ0028.1+3103	00 : 28 : 10	+31 : 03 : 48.1	10.6	138	0.46	8.7	17.48
NGC513	01 : 24 : 26	+33 : 47 : 57.9	11.1	145	0.48	7.0	17.39
KAZ238	00 : 00 : 58	+33 : 20 : 38.5	11.5	149	0.50	9.0	17.50
MRK1158	01 : 34 : 59	+35 : 02 : 22.1	12.0	156	0.52	7.7	17.43
2MASSJ00413+2816	00 : 41 : 18	+28 : 16 : 40.8	13.0	169	0.56	10.6	17.57
FBS0150+396	01 : 53 : 06	+39 : 55 : 45.2	13.4	174	0.58	9.3	17.51
3C48	01 : 37 : 41	+33 : 09 : 35.1	13.6	176	0.59	14.8	17.71
4C25.01	00 : 19 : 39	+26 : 02 : 52.3	16.0	206	0.69	7.0	17.39
PG0052+251	00 : 54 : 52	+25 : 25 : 38.9	16.0	207	0.69	6.9	17.38
2MASSJ00294+2424	00 : 29 : 24	+24 : 24 : 29.0	17.1	220	0.74	10.7	17.57
RXSJ015536.7+311525	01 : 55 : 36	+31 : 15 : 17.0	17.7	228	0.76	6.8	17.37
RBS2055	23 : 51 : 52	+26 : 19 : 32.5	18.3	235	0.79	6.1	17.33
RBS2061	23 : 55 : 48	+25 : 30 : 31.6	18.5	238	0.80	6.0	17.32
3C66A	02 : 22 : 39	+43 : 02 : 07.8	18.5	239	0.80	12.6	17.64
RXJ0053.7+2232	00 : 53 : 46	+22 : 32 : 22.1	18.9	243	0.81	6.6	17.36
MRK930	23 : 31 : 58	+28 : 56 : 49.9	18.9	244	0.81	5.6	17.29
RXJ0048.7+2127	00 : 48 : 45	+21 : 27 : 15.9	19.9	255	0.85	12.0	17.62
MRK357	01 : 22 : 40	+23 : 10 : 14.7	19.9	256	0.85	8.2	17.46
3C59	02 : 07 : 02	+29 : 30 : 45.9	20.7	266	0.89	11.9	17.62
PG0117+213	01 : 20 : 17	+21 : 33 : 46.2	21.2	272	0.91	6.3	17.34
HS0137+2329	01 : 40 : 35	+23 : 44 : 51.0	21.3	272	0.91	6.7	17.37
KUV02196+3253	02 : 22 : 31	+33 : 06 : 21.2	21.4	274	0.91	6.7	17.37
RXJ0029.0+1957	00 : 29 : 03	+19 : 57 : 10.0	21.5	275	0.92	7.9	17.44
RXJ0044.9+1921	00 : 44 : 59	+19 : 21 : 41.0	21.9	280	0.94	9.9	17.54
MRK335	00 : 06 : 19	+20 : 12 : 10.5	22.4	287	0.96	9.6	17.52
UGC1098	01 : 32 : 16	+21 : 24 : 38.9	22.4	287	0.96	9.4	17.52
RXSJ023231.4+340435	02 : 32 : 33	+34 : 04 : 27.9	22.8	291	0.97	9.7	17.53
RXSJ225148.5+341937	22 : 51 : 47	+34 : 19 : 28.9	22.9	292	0.97	10.1	17.55
MRK1148	00 : 51 : 54	+17 : 25 : 58.4	23.9	304	1.02	6.4	17.35
RBS2005	23 : 25 : 54	+21 : 53 : 14.0	25.2	320	1.07	8.0	17.44
MRK1179	02 : 33 : 22	+27 : 56 : 13.1	26.2	332	1.11	9.2	17.51

Table 1 continued on next page

Table 1 *(continued)*

QSO name	RA (J2000)	Dec (J2000)	$\Delta\theta$[a] (°)	ρ[b] (kpc)	ρ/R_{vir}[c]	σ_b[d] (mK)	log N(H I)[e] (5σ sens.)
PG0003+158	00 : 05 : 59	+16 : 09 : 49.0	26.3	333	1.11	9.6	17.52
BLANK	22 : 42 : 39	+29 : 43 : 31.5	26.8	339	1.13	9.1	17.50

[a] Anglular separation from the center of M31.

[b] We adopt 752 kpc as the distance of M31 from the sun (Riess et al. 2012).

[c] We assume $R_{\rm vir} = 300$ kpc following Lehner et al. (2015).

[d] RMS brightness temperature noise per 0.6 km s^{-1} channel.

[e] The 5σ column density sensitivities (in cm^{-2}) for each sight line. Any detections are summarized in Table 2.

Table 2. H I Detections

QSO Name	ρ (kpc)	log N(H I) [cm^{-2}]	$\langle v_{\rm LSR}\rangle$ (km s^{-1})	FWHM (km s^{-1})
RBS2055	235	17.88 ± 0.05	-331.5 ± 1.0	25.1 ± 2.3
RBS2061	238	17.79 ± 0.08	-334.0 ± 1.7	29.1 ± 4.0

Table 3. H I Covering Factors

ρ (kpc)	$\rho/R_{\rm vir}$	$f_c(\leq \rho)$[a]	N[b]
50	0.17	< 0.369	4
75	0.25	< 0.250	7
100	0.33	< 0.162	12
125	0.42	< 0.142	14
150	0.50	< 0.114	18
175	0.58	< 0.099	21
200	0.67	< 0.095	22
225	0.75	< 0.085	25
250	0.83	< 0.069	31
275	0.92	< 0.057	38
300	1.00	< 0.051	43
325	1.08	< 0.049	45
350	1.17	< 0.046	48

[a] Upper limits are at 90% confidence.

[b] Number of sight lines considered in covering factor determination.

Table 4. H I Covering Factors with MS Detections

ρ (kpc)	$\rho/R_{\rm vir}$	$f_c(\leq \rho)_{0.1}$[a]	$f_c(\leq \rho)_{0.5}$[a]	$f_c(\leq \rho)_{0.9}$[a]	N[b]
250	0.83	0.035	0.083	0.158	31
275	0.92	0.029	0.068	0.131	38
300	1.00	0.025	0.060	0.116	43
325	1.08	0.024	0.058	0.112	45
350	1.17	0.023	0.054	0.105	48

[a] The 10%, 50% (median), and 90% quantiles for the H I covering factors assuming the probable MS detections are associated with M 31.

[b] Number of sight lines considered in covering factor determination.